

# Superflare on a rapidly-rotating solar-type star captured in X-rays

Andrey Mukhin<sup>a,b,\*</sup>, Roman Krivonos<sup>a</sup>, Ilfan Bikmaev<sup>c,d</sup>, Mark Gorbachev<sup>c</sup>, Irek Khamitov<sup>c</sup>, Sergey Sazonov<sup>a</sup>, Marat Gilfanov<sup>a,e</sup>, Rashid Sunyaev<sup>a,f</sup>

<sup>a</sup>Space Research Institute (IKI), Russian Academy of Sciences, Moscow, 117997, Russia

<sup>b</sup>Moscow Institute of Physics and Technology (National Research University), , Moscow, 117303, Russia

<sup>c</sup>Kazan Federal University, Kremlevskaya Str.18, Kazan, 420008, Russia

<sup>d</sup>Academy of Sciences of Tatarstan Republic, Baumana Str. 20, Kazan, 420111, Russia

<sup>e</sup>Max-Planck-Institut für Astrophysik, Karl-Schwarzschild-Str. 1, Garching, D-85741, Germany

<sup>f</sup>Institute for Advanced Study, 1 Einstein Drive, Princeton, 08540, New Jersey, USA

## Abstract

In this work, we studied X-ray source SRGe J021932.4–040154 (SRGe J021932), which we associated with a single X-ray active star of spectral class G2V–G4V and the rotational period  $P_{\text{rot}} < 9.3$  days. Additional analysis of TESS light-curves allowed for the rotational period estimation of  $3.2 \pm 0.5$  days. SRGe J021932 was observed with the *SRG/eROSITA* during eUDS survey in 2019 in a much dimmer state compared to the *XMM-Newton* catalogue 4XMM-DR12. Detailed analysis revealed that the archival *XMM-Newton* observations captured the source during a flaring event in 2017. The *XMM-Newton* light curve demonstrates a strong flare described with the Gaussian rise and exponential decay, typical for stellar flares, characterized by timescales of  $\sim 400$  s and  $\sim 1300$  s, respectively. The spectral analysis of the quiescent state reveals  $\sim 10$  MK plasma at luminosity of  $(1.4 \pm 0.4) \times 10^{29}$  erg s $^{-1}$  (0.3–4.5 keV). The spectrum of the flare is characterized by temperature of  $\sim 40$  MK and luminosity  $(5.5 \pm 0.6) \times 10^{30}$  erg s $^{-1}$ . The total energy emitted during the flare  $\sim 1.7 \times 10^{34}$  erg exceeds the canonical threshold of  $10^{33}$  erg, allowing us to classify the observed event as a superflare on a rapidly-rotating solar-type star. Additionally, we present the upper limit on the surface starspot area based on the brightness variations and consider the hypothesis of the object being a binary system with G-type and M-type stars, suggested by two independent estimations of radial velocity variations from APOGEE-2 and *Gaia*.

**Keywords:** X-rays: stars, stars: activity, stars: flare, stars: solar-type

## 1. Introduction

Solar flares are powerful magnetic phenomena caused by the reconnection of magnetic lines in the solar corona with rapid release of magnetic energy (Fletcher et al., 2011). This process leads to effective acceleration of electrons, that propagate downwards to the chromosphere, causing the heating of surrounding plasma up to millions degrees K. The pressure of heated plasma soon exceeds the pressure of chromosphere, leading to the expansion of the plasma and creation of a region of hot (with temperatures  $> 10$  MK) optically thin large volume of plasma, that eventually cools down to the usual stellar coronae temperature of 1–3 MK (Benz and Güdel, 2010). Different stages of the process have been observed in all wavelengths from radio to  $\gamma$ -rays, however, the emission of hot region and the solar corona is most prominent in X-rays.

On the one hand, the solar flares allow us to study in details the stellar flares on G-dwarf stars, on the other hand, the investigation of stellar flares on distant G-dwarfs can reveal more extreme events, potentially being observed on the Sun. While the solar flares typically release  $10^{29} - 10^{32}$  erg in optical range at the timescale of several hours, some G-dwarfs were observed

to demonstrate flaring events with energy release of  $10^{33} - 10^{36}$  erg, often called as “superflares” (Schaefer et al., 2000; Maehara et al., 2012, 2015; Tu et al., 2021).

Superflares were already observed for a variety of stellar objects besides solar-type G-dwarfs: the RS CVn binaries (See, for example), young T Tauri stars, and UV Ceti-like red dwarfs (Haisch et al., 1991). Superflares in X-ray range, however, were observed only for several objects: Algol (Favata and Schmitt, 1999), AB Doradus (Maggio et al., 2000; Didel et al., 2024), II Pegasi (Osten et al., 2007), EV Lac (Favata et al., 2000; Osten et al., 2010), CC Eri (Karmakar et al., 2017), UX Arietis (Franciosini et al., 2001), DG CVn (Fender et al., 2015), SZ Psc (Karmakar et al., 2023), and some of them were even captured simultaneously in optical and X-ray range: AD Leonis (XMM-Newton and TESS, Stelzer et al., 2022), ten K-M, one F9 and one G8 star in the Pleiades (XMM-Newton and Kepler/K2, Guarcello et al., 2019) and three more K-M stars using XMM-Newton and Kepler (Kuznetsov and Kolotkov, 2021).

The majority of the hosts for these X-ray superflares turned out to be either M-stars or binary, or multiple systems with an M-component (Karmakar et al., 2022), however, there are examples of G-dwarf stars with superflares both in optical and X-ray range with no observed companions or in wide binary systems: EK Draconis (Namekata et al., 2024),  $\kappa^1$  Ceti (Hamaguchi et al., 2023) and several others (Audard et al., 2000;

\*Corresponding author

Email address: amukhin@cosmos.ru (Andrey Mukhin)

Schaefer et al., 2000; Shibata et al., 2013).

In this study, we investigate the weak X-ray source SRGe J021932.4–040154 (hereafter SRGe J021932) detected during the SRG/eROSITA (Sunyaev et al., 2021; Predehl et al., 2021) X-ray survey of the UKIDSS Ultra Deep Survey field (eUDS, Krivonos et al., 2024), that was previously observed in much brighter X-ray state on January 1 2017 with XMM-Newton under the name 4XMM J021932.−040153 (4XMM-DR12 catalogue, Webb et al., 2020). SRGe J021932 is associated with an optical G-dwarf star with no confirmed companions by several observatories. We reconstructed the XMM-Newton light-curve, which revealed the rapid increase in the flux followed by gradual decay, implying the possible flaring nature. By the observed total energy emission of  $10^{34}$  erg and X-ray luminosity of  $\approx 10^{30}$  erg s $^{-1}$  in 0.3–4.5 keV band, we classify this event as a superflare. We present XMM-Newton timing and spectral analysis of SRGe J021932 in quiescent (non-flaring) state observed in 2016 and during the superflare captured in 2017, as well as SRG/eROSITA observations in 2019.

## 2. Identification of SRGe J021932

Krivonos et al. (2024) report that X-ray emission of SRGe J021932 is consistent with a point-like object (RA=2:19:32.523, Dec=−4:01:53.671, J2000), and its position is determined with 2.4'' uncertainty (*RADEC\_ERR*). We consider an association as likely if the optical position is within  $1.5 \times RADEC\_ERR$ , which approximately corresponds to 90% position error. We performed search within this error radius in the catalogues of *Gaia* (Gaia Collaboration et al., 2016), Transiting Exoplanet Survey Satellite (TESS, Ricker et al., 2015) and APOGEE–2 of SDSS (Blanton et al., 2017). The following counterparts have been found: *Gaia* DR3 2489887138146547456 (Gaia Collaboration et al., 2023) with 2.17'' separation, TIC 332890423 from TESS Input Catalogue v8.0 (TIC-8) (Stassun et al., 2019) with 2.54'' separation and APOGEE ID 2M02193235–0401533 from APOGEE–2 SDSS DR17 (Abdurro'uf et al., 2022) with 2.59'' separation. All three associations' coordinates are consistent with each other within 0.4'', thus we assume them to be the observations of the same object 2MASS J02193235-0401533. All three catalogs report that the position of SRGe J021932 is consistent with a star.

### 2.1. Optical properties of the star

Table 1 outlines the properties of all three associations, namely, effective temperature  $T_{\text{eff}}$ , estimated distance, radial velocity RV, rotational velocity radial component  $v \sin i$ , surface gravity  $\log g$ , [M/H] metallicity compared to Solar, radius, mass and bolometric luminosity of the object.

The effective temperature indicates the associated star to be G2–G4 spectral class. The surface gravity and the estimated radius are typical for the main sequence stars. Thus, we assume that SRGe J021932 is an X-ray active yellow dwarf (G2V–G4V) at  $\approx 347$  pc from Earth.

### 2.2. Binary system indications

Although the 2MASS J02193235-0401533 is not reported as a binary system by any of the used catalogs, it should be noted, that there are two peculiar features present in APOGEE-2 SDSS DR17 and *Gaia* DR3 data, that can indicate a presence of a companion of the G-star.

APOGEE-2 SDSS DR17 reports the radial velocity to be determined with the uncertainties of 0.04 km s $^{-1}$ , while the scatter of individual visits around average radial velocity is reported to be 0.53 km s $^{-1}$ . The scatter of the individual visits much larger than typical uncertainties can be used as an indicator of radial velocity variations due to being in a binary system. Nevertheless, only 3 data points for the radial velocity estimation are currently present in APOGEE-2 SDSS DR17, and further observations are required to reliably detect variations.

*Gaia* DR3 estimations based on 12 transits show the radial velocity variation amplitude of 17.5 km s $^{-1}$  despite the estimated uncertainties of only 1.6 km s $^{-1}$ . As well as for the SDSS, it can indicate radial velocity variability and the presence of the companion. As the radial velocity time series is not currently available, we estimate the probability of the radial velocity variations with the reported P-value for constancy of 0.64. While it cannot be used to reject neither the binary system hypothesis nor the single star hypothesis, we interpret the reported statistics to imply no significant radial velocity variations are observed.

Thus, in this work, we assume the SRGe J021932 to be a single star, although further analysis is required to make a reliable conclusion.

## 3. X-ray Observations

SRGe J021932 was observed with SRG/eROSITA in eUDS survey (Krivonos et al., 2024) conducted in August–September 2019 during the SRG Calibration and Performance Verification (Cal-PV) phase. The source attracted attention by its very dim flux compared to the XMM-Newton archival observations as reported in 4XMM-DR12 catalogue (Webb et al., 2020).

### 3.1. SRG/eROSITA

The processing of the SRG/eROSITA data was performed using the eSASS version 211201 software as described in Krivonos et al. (2024). We ran the `srctool` task in AUTO mode (when `srctool` generates source and background regions automatically) to extract spectral information between 0.2 and 10 keV of all eUDS sources, including SRGe J021932. The source regions are circles and the background regions are annuli, both centered on the position of the source. The size of the regions is selected taking the source counts, the level of the background, the best fitting source extent model radius, and other parameters into account<sup>1</sup>. The result of the automatic generation of source and background regions is shown in Fig. 1. The source spectrum is extracted from the circle with  $R = 43''$

<sup>1</sup>See the eSASS documentation at <https://erosita.mpe.mpg.de/edr>

| Property                      | <i>Gaia</i> DR3    | TIC-8             | APOGEE-2 DR17      |
|-------------------------------|--------------------|-------------------|--------------------|
| $T_{\text{eff}}$ , K          | $5736 \pm 7$       | $5760 + 120$      | $5678 \pm 26$      |
| Distance, pc                  | $347 \pm 5$        | $342 \pm 12$      | –                  |
| RV, km s $^{-1}$              | $19.14 \pm 1.58$   | –                 | $20.18 \pm 0.04$   |
| v sin <i>i</i> , km s $^{-1}$ | –                  | –                 | 5.78               |
| log g, cm s $^{-2}$           | $4.3296 \pm 0.008$ | $4.38 \pm 0.08$   | $4.18 \pm 0.02$    |
| [M/H]                         | $-0.232 \pm 0.007$ | $0.004 \pm 0.014$ | $-0.024 \pm 0.005$ |
| Radius, $R_{\odot}$           | $1.04 \pm 0.01$    | $1.09 \pm 0.06$   | –                  |
| Mass, $M_{\odot}$             | $1.0 \pm 0.4$      | $1.0 \pm 0.1$     | –                  |
| Luminosity, $L_{\odot}$       | $1.19 \pm 0.04$    | $1.18 \pm 0.09$   | –                  |

Table 1: Properties of SRGe J021932 associations with *Gaia* DR3 (Gaia Collaboration et al., 2023), TESS Input Catalogue v8.0 (Stassun et al., 2019) and APOGEE-2 SDSS DR17 (Abdurro’uf et al., 2022).

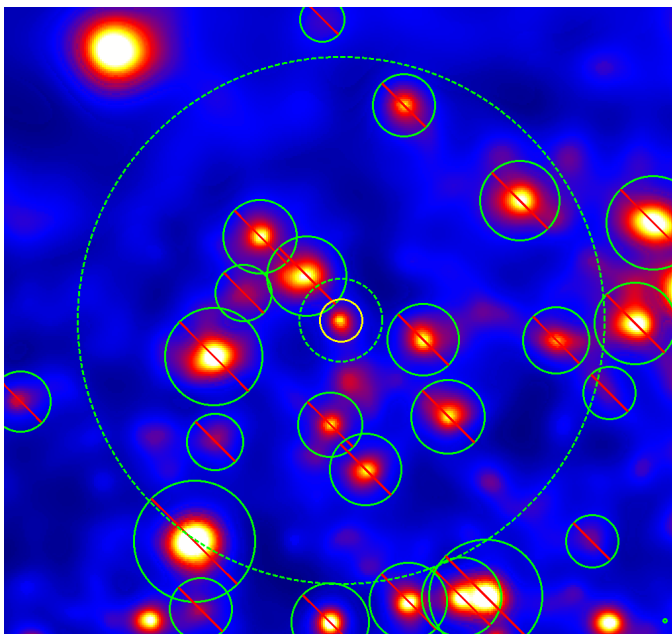


Figure 1: *SRG/eROSITA* 0.3–2.3 keV sky map of the region around SRGe J021932 (in the center) in the units of cts s $^{-1}$ . The exposure-corrected image has been adaptively smoothed with the *dmimgadapt* task from CIAO-4.15 (Fruscione et al., 2006) using a Gaussian kernel. The image is shown in the square-root scale colour map, (“b” in DS9 notation, see Joye and Mandel, 2003) ranging from zero (black) to 0.001 and above (white). The X-ray spectrum of SRGe J021932 has been extracted from yellow  $R = 43''$  circle. The background has been estimated in annulus region  $R_{\text{min}} = 84''$  and  $R_{\text{max}} = 530''$ . The excluded regions are marked by a crossed out circles.

around the best-fit source position. The total count within this aperture is 44 over an exposure of 4.1 ks. As seen from the figure, despite the crowded field around SRGe J021932, it is not affected by spatial confusion with nearby sources.

Additionally, SRGe J021932 is present in the *SRG/eROSITA* catalog of X-ray sources in the eastern Galactic hemisphere based on the  $\sim$ 4.4 *SRG* all sky surveys (December 2019 to February 2022) (Khamitov et al., 2022). The source was detected with DET\_LIKE = 10.2 and a single optical *Gaia* DR3 catalog association inside  $R_{\text{98}} = 14.3''$ . The X-ray luminosity of the source in 0.3–2.3 keV based on the *SRG/eROSITA* flux and *Gaia* parallax data is estimated as  $(2.2 \pm 0.8) \times 10^{29}$  erg s $^{-1}$ .

| ObsID      | Date       | Time (UTC)          | T (ks) |
|------------|------------|---------------------|--------|
| 0785100401 | 2016-07-03 | 03:44:16 - 09:50:56 | 22     |
| 0793580201 | 2017-01-01 | 07:02:08 - 09:32:08 | 9      |

Table 2: *XMM-Newton* observations of the SRGe J021932 used in this work.

### 3.2. *XMM-Newton*

We use two observations of *XMM-Newton* (Jansen et al., 2001): ObsID 0785100401 on July 3 2016 and ObsID 0793580201 on January 1 2017 (Table 2) conducted as a part of the *XMM-SERVS* survey (Chen et al., 2018). Since MOS1 camera was not operating during both observations, we used data from PN and MOS2 cameras only.

The *XMM-Newton* observations were processed using the *XMM-Newton* Science Analysis System (SAS) v21.0.0 software. The observations were filtered for the flaring particle background, and the light-curves and spectra were generated using standard SAS Data Analysis Threads with default selection parameters for PN (PATTERN $\leq$ 4) and MOS2 (PATTERN $\leq$ 12). We extracted light-curves and spectra from the source region described with  $R = 30''$  circle around SRGe J021932 position and the background from the 45 – 90'' annulus as shown in Fig. 2. The images are extracted with the same filtering parameters as the spectra and light-curves. The black streaks observed for the PN camera represent the edges of detectors (Strüder et al., 2001) and are taken into account in the standard XMM data processing tools.

## 4. Analysis and results

As seen from the sky images presented in Fig. 2, *XMM-Newton* captured SRGe J021932 in two different states – in 2016 it was observed being much dimmer and in 2017 being brighter for both cameras. Hereafter, we refer to the state observed during 2016 as a quiescent state and the state during 2017 as a flaring state.

### 4.1. Light-curve analysis

Assuming no significant variations within 20 ks exposure time ( $\approx$ 5 hours) during the quiescent state, we fit the 2016 light-curves of SRGe J021932 with a constant. The resulting values for constant count rates are  $(1.2 \pm 0.5) \times 10^{-2}$  cts s $^{-1}$  and  $(1.4 \pm 1.3) \times 10^{-3}$  cts s $^{-1}$  for PN and MOS2, respectively.

|                                    | PN                                 | MOS2                                |
|------------------------------------|------------------------------------|-------------------------------------|
| $C_{\text{const}}$ , cts s $^{-1}$ | $2.3^{+1.7}_{-1.2} \times 10^{-2}$ | $-0.1^{+0.3}_{-0.3} \times 10^{-2}$ |
| $A_{\text{flare}}$ , cts s $^{-1}$ | $4.6^{+1.2}_{-0.7} \times 10^{-1}$ | $1.3^{+0.3}_{-0.3} \times 10^{-1}$  |
| $t_{\text{peak}}$ , s              | $3.1^{+0.1}_{-0.2} \times 10^3$    | –                                   |
| $\tau_{\text{rise}}$ , s           | $4.1^{+1.4}_{-3.5} \times 10^2$    | –                                   |
| $\tau_{\text{decay}}$ , s          | $1.3^{+0.6}_{-0.4} \times 10^3$    | –                                   |
| $\chi^2/\text{dof}$                | 0.79/40                            | 0.94/36                             |

Table 3: Table of best-fit flare model parameters for XMM2 PN and MOS2 light-curves with 90% confidence intervals calculated via bootstrapping. Empty cells in the second column correspond to the fixed parameters taken from PN model. Value of  $t_{\text{peak}}$  is calculated from the beginning of the PN camera observation.

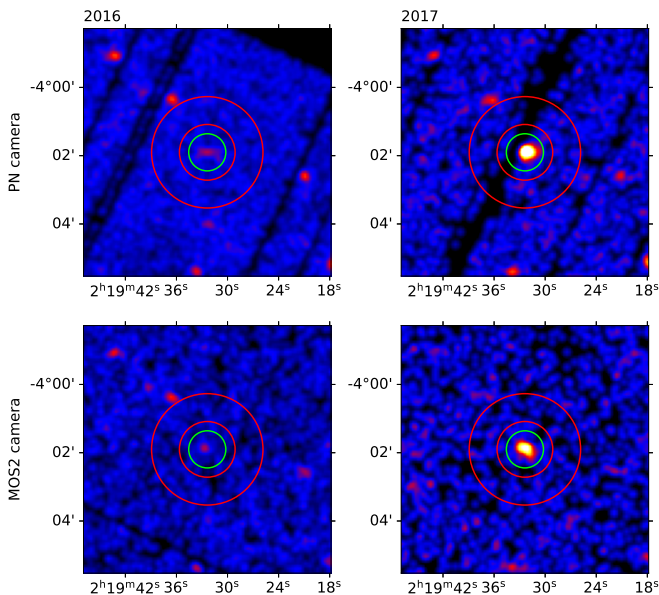


Figure 2: *XMM-Newton* sky images around SRGe J021932 in cts s $^{-1}$  with PN (top row, 0.2–15 keV) and MOS2 (bottom row, 0.2–10 keV) cameras for two *XMM-Newton* observations from 2016 (left column) and 2017 (right column) observations as described in Table 2. Images in each row are shown with the matching square-root scale colour maps “b” in DS9 notation, ranging from  $10^{-6}$  to  $10^{-3}$  for PN and from  $10^{-6}$  to  $5 \times 10^{-4}$  for MOS2. All images were smoothed with the Gaussian kernel ( $\sigma = 1$  pix). The X-ray spectrum and light-curves for the SRGe J021932 have been extracted from the green circle region with  $R = 30''$ . Red annulus ( $R_{\text{in}} = 45''$  and  $R_{\text{out}} = 90''$ ) represents the region of background estimation.

For 2017 observation, the light-curves in both cameras show a rapid rise and gradual decay, which we fit as a sum of a constant count rate and an asymmetric peak with Gaussian rise and exponential decay. Thus, the model for fitting the light-curves of the flare is:

$$C(t) = C_{\text{const}} + A_{\text{flare}} \times \begin{cases} \exp\left(-\left(\frac{t-t_{\text{peak}}}{\tau_{\text{rise}}}\right)^2\right), & t \leq t_{\text{peak}} \\ \exp\left(-\frac{t-t_{\text{peak}}}{\tau_{\text{decay}}}\right), & t > t_{\text{peak}} \end{cases} \quad (1)$$

where  $C_{\text{const}}$  is the constant count rate,  $A_{\text{flare}}$  is the amplitude of the flare,  $t_{\text{peak}}$  is the time position of the flare peak,  $\tau_{\text{rise}}$  and  $\tau_{\text{decay}}$  are the estimations rise and decay phase characteristic times, respectively.

For PN light-curve we fitted the data with the model with five free parameters ( $C_{\text{const}}$ ,  $A_{\text{flare}}$ ,  $t_{\text{peak}}$ ,  $\tau_{\text{rise}}$ ,  $\tau_{\text{decay}}$ ). MOS2 light-curve, due to poor statistics, was fitted with two free parameters  $C_{\text{const}}$ ,  $A_{\text{flare}}$  and other parameters fixed to the optimal values found for PN light-curve.

The best-fit parameters of the flare light-curves with estimated 90% confidence intervals are presented in Table 3. The resulting model together with PN and MOS2 light-curves are shown in Fig. 3.

The estimated constant level count rates for 2017 observation are consistent with the constant count rates for 2016 observation. The rise and decay phases are characterized by  $4.1^{+1.4}_{-3.5} \times 10^2$  s and  $1.3^{+0.6}_{-0.4} \times 10^3$  s.

We determined the nominal start of the flare ( $T_{\text{start}} = 599646020$  s or 2017 January 1 08:19:11 UTC) as the time when the best-fit flare model (Eq. 1) exceeds 1% of the peak value  $A_{\text{flare}}$ . In the following, we extract X-ray spectrum of the flare after this time.

#### 4.2. Spectral analysis

For the spectral analysis, we have used a total of five spectra:

- two, PN and MOS2, spectra in quiescent state (2016)
- two, PN and MOS2, spectra in flaring state (2017)
- a single *SRG/eROSITA* spectrum in quiescent state (2019)

The 2017 spectra are extracted within the time interval between  $T_{\text{start}}$  (Sect. 4.1) and the end of observation, resulting in a total

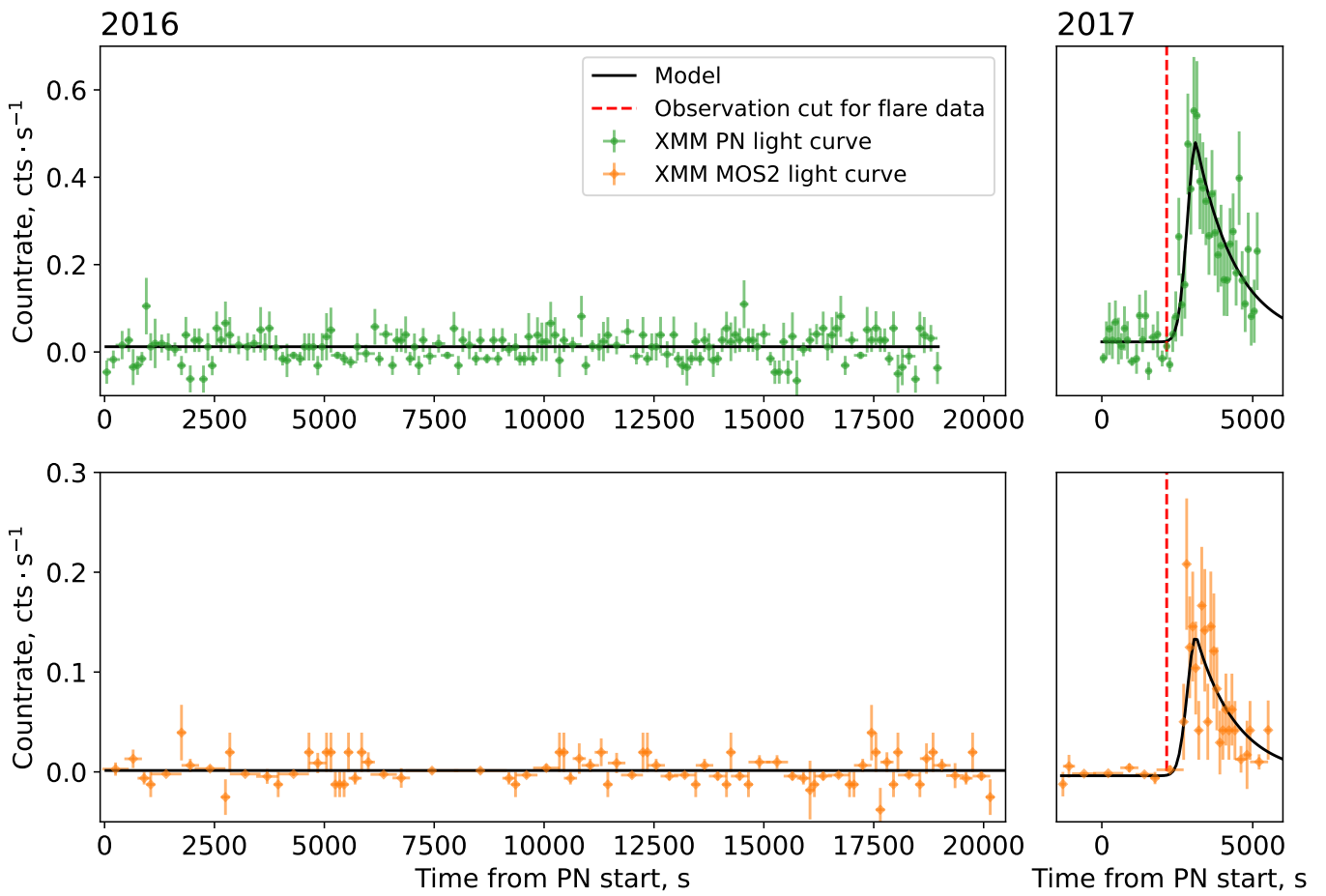


Figure 3: Light-curves of the source from XMM-Newton PN (top row) and MOS2 (bottom row) cameras for observations in the quiescent state (2016, left column) and during the flare (2017, right column). The black line represents the flare light-curve model described by the Eq. 1. Red vertical dashed line shows the position of the estimated start of the flare.

|              | $\Gamma$      | Flux (0.3–4.5 keV)<br>erg s <sup>-1</sup> cm <sup>-2</sup> | cstat / bins |
|--------------|---------------|--|--------------|
| 2016 PN      | $1.6 \pm 0.4$ | $1.7^{+0.6}_{-0.5} \times 10^{-14}$                        | 59.19 / 56   |
| 2016 MOS2    | $2.4 \pm 0.7$ | $1.4^{+0.8}_{-0.7} \times 10^{-14}$                        | 21.95 / 20   |
| 2017 PN      | $1.7 \pm 0.2$ | $(4.3 \pm 0.6) \times 10^{-13}$                            | 55.42 / 47   |
| 2017 MOS2    | $1.6 \pm 0.3$ | $(3.2 \pm 0.6) \times 10^{-13}$                            | 33.09 / 30   |
| 2019 eROSITA | $2.0 \pm 0.6$ | $1.5^{+0.8}_{-0.6} \times 10^{-14}$                        | 39.59 / 31   |

Table 4: Results of fitting of 5 X-ray SRGe J021932 spectra with a simple powerlaw model with the fixed galactic neutral hydrogen column density absorption (tbabs(powerlaw)).

exposure of 3050 s. All spectra were re-binned to contain at least 3 counts in a bin to perform fitting with Cash statistics (Cash, 1979). For the spectral fitting, we used XSPEC (Arnaud, 1996) software.

For the initial spectral analysis, we have fitted all 5 spectra separately with a simple power law model with fixed galactic neutral atomic hydrogen (NHI) column density  $1.91 \times 10^{20} \text{ cm}^{-2}$  derived by HI4PI Collaboration et al. (2016). We use the complete column density estimation as the SRGe J021932 is situated at a high galactic latitude ( $b \sim -59^\circ$ ) and the distance of 343 pc. We then calculated the estimated flux in 0.3–4.5 keV range for every spectrum. The resulting values are presented in Table 4.

The X-ray spectrum of SRGe J021932 observed by SRG/eROSITA in 2019 is consistent with PN/MOS2 spectra in 2016, while showing significant deviation in PN/MOS2 flux in 2017. We assume that XMM-Newton and SRG captured SRGe J021932 in the quiescent state in 2016 and 2019, respectively.

For the spectral analysis of the SRGe J021932 in quiescent state, we combined 2016 and 2019 observations. Due to poor statistics, we assumed all three spectra to be described with a single model, consisting of the one-temperature plasma emission model (APEC, Smith et al., 2001) modified by galactic hydrogen column density absorption (TBabs). The galactic absorption is fixed to  $1.91 \times 10^{20} \text{ cm}^{-2}$ , the abundance of the plasma is set free and the redshift is fixed to zero. The best-fitting parameters with estimated 90% confidence intervals are listed in Table 5 and the spectrum with a model is shown in Figure 4. The temperature of the plasma in the quiescent state is estimated as  $(0.8^{+0.8}_{-0.2} \text{ keV})$  or  $(9.3^{+9.3}_{-2.3} \times 10^6 \text{ K})$ . The emission measure in the quiescent state is estimated as  $(2.4 \pm 1.0) \times 10^{52} \text{ cm}^{-3}$ . The abundance for the quiescent state is  $0.06^{+0.11}_{-0.03} Z_\odot$ . Based on the estimated unabsorbed flux in 0.3–4.5 keV range of  $(1.0 \pm 0.3) \times 10^{-14} \text{ erg s}^{-1} \text{ cm}^{-2}$  and the distance to SRGe J021932 of  $347 \pm 5 \text{ pc}$  we can estimate the unabsorbed X-ray luminosity in 0.3–4.5 keV range as  $L_{XQ} = (1.4 \pm 0.4) \times 10^{29} \text{ erg s}^{-1}$ .

Similarly, PN/MOS2 flare spectrum in 2017 was fitted with one-temperature plasma model with fixed galactic absorption and free abundance (Table 5 and Figure 5). The spectrum is characterized by the hot plasma component with the estimated temperature of  $3.4^{+1.4}_{-0.9} \text{ keV}$  (or  $3.9^{+1.6}_{-1.0} \times 10^7 \text{ K}$ ) and emission measure of  $(5.2 \pm 1.0) \times 10^{53} \text{ cm}^{-3}$ . The abundance during the flare was only estimated with the upper limit as the value <

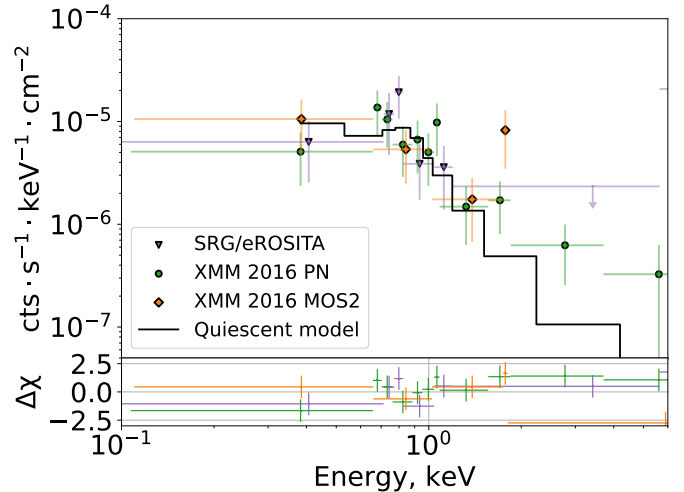


Figure 4: Quiescent X-ray spectrum of SRGe J021932 based on the SRG/eROSITA, XMM 2016 PN and XMM 2016 MOS2 observations. Black solid line shows the best-fit model spectrum.

|  | Quiescent state                       | Flaring state                         |
|--|---------------------------------------|---------------------------------------|
| $N_H, \text{ cm}^{-2}$                     | $1.91 \times 10^{20} \text{ (fixed)}$ | $1.91 \times 10^{20} \text{ (fixed)}$ |
| $kT, \text{ keV}$                          | $0.8^{+0.8}_{-0.2}$                   | $3.4^{+1.4}_{-0.9}$                   |
| $\text{EM}, \text{ cm}^3$                  | $(2.4 \pm 1.0) \times 10^{52}$        | $(5.2 \pm 1.0) \times 10^{53}$        |
| $Z, Z_\odot$                               | $0.06^{+0.11}_{-0.03}$                | $< 0.82$                              |
| Flux, erg s <sup>-1</sup> cm <sup>-2</sup> | $(1.0 \pm 0.3) \times 10^{-14}$       | $(3.8 \pm 0.4) \times 10^{-13}$       |
| cstat / dof                                | 102.7 / 91                            | 86.3 / 73                             |

Table 5: Results of spectral fitting using the single-temperature plasma models with fixed galactic column density for the spectra in quiescent and flaring states. The values are shown with 90% confidence intervals. The unabsorbed flux is calculated in 0.3–4.5 keV range.

$0.82 Z_\odot$ . The estimated unabsorbed luminosity of the flare is estimated as  $L_{XF} = (5.5 \pm 0.6) \times 10^{30} \text{ erg s}^{-1}$ . The total energy emitted during the flare in 0.3–4.5 keV, assuming the constant temperature during the flare, can be estimated as  $E_X = (1.7 \pm 0.2) \times 10^{34} \text{ erg}$ .

## 5. Discussion

The spectral analysis of SRGe J021932 in the quiescent state revealed new indirect estimates for the stellar parameters. Both the emission measure and temperature in the quiescent state are in agreement with the values reported in Takasao et al. (2020) from the sample of 10 X-ray active G-dwarfs, however, the estimated quiescent luminosity of our star lies somewhat in between the two sample subdivisions to X-ray bright G-dwarfs and other Solar-type stars.

The X-ray luminosity of the SRGe J021932 in quiescent state is  $\sim 2$  orders of magnitude higher compared to the Sun, which can be expected from the relatively young (0.6 Gyr) solar-type stars (Güdel et al., 1997), such as, for example, 9 Ceti (BE Cet) (Ra=00:22:51.7884553555, Dec=−12:12:33.969921319, J2000). Thus, the SRGe J021932 is likely a young active star with age of  $< 1$  Gyr.

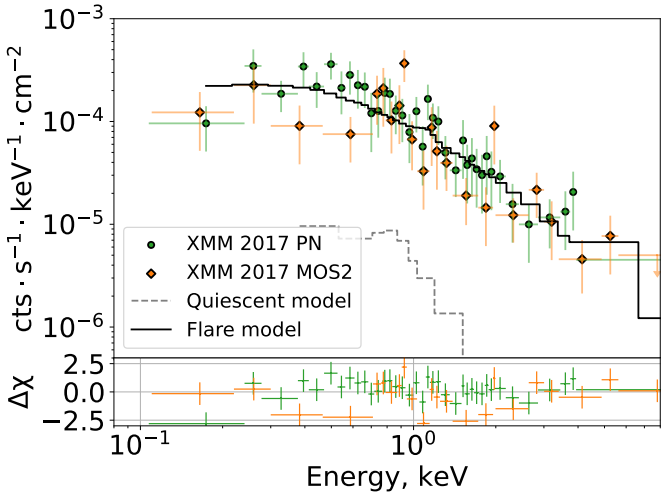


Figure 5: Flare X-ray spectrum of SRGe J021932 based on the XMM 2017 PN and XMM 2017 MOS2 observations. Black solid line shows the best-fit flare model spectrum. Dashed grey line shows the quiescent model for comparison.

For direct comparison with the *SRG/eROSITA* all sky survey catalog, we recalculated the X-ray luminosity in the quiescent state in 0.3–2.3 keV range. The resulting value of  $1.4^{+0.5}_{-0.3} \times 10^{29}$  erg s $^{-1}$  is in agreement with the luminosity based on the 4.4 all sky surveys ( $2.2 \pm 0.8 \times 10^{29}$  erg s $^{-1}$ ). Thus, two independent *SRG/eROSITA* observations of the SRGe J021932 show no significant luminosity variations or Sun-like cycle activity across the 3-year span.

The estimated fluxes in the quiescent and flaring states show the  $\sim 38$  times increase in flux. In this work, we assume that the estimation of the flux in the flaring state describes the flux of the flare itself, neglecting the contribution of the stellar flux of the SRGe J021932 from outside the active region. In case the flux from outside the active region can be described by the flux in the quiescent state, it contributes less than 3% of the observed flux during the flaring state. Thus, we assume that the spectrum, flux and luminosity estimations can be interpreted as the parameters dominated by the flare itself.

The total X-ray energy emission  $E_X = (1.7 \pm 0.2) \times 10^{34}$  erg during the flare of SRGe J021932 exceeds  $10^{33}$  erg, the canonical threshold for the superflares classification (Schaefer et al., 2000). Moreover, the simultaneous observations of superflares in optical and X-ray ranges (Guarcello et al., 2019) show that the total emitted energy in optical range is similar or even exceeds the total energy emitted in X-rays, so the bolometric energy emission during the flare of SRGe J021932 can be expected to be several times bigger than observed in X-rays. Thus, we confirm the classification of the observed event as a superflare on G-type star. The parameters of the superflare are in agreement with the analysis of a sample of X-ray stellar flares on cool (F-M spectral class) stars (Pye et al., 2015).

### 5.1. Abundance estimation

Abundance in the quiescent state is significantly sub-Solar but is in agreement with the abundances found from the low-resolution spectral analysis of the sample of X-ray active G-

dwarfs (Takasao et al., 2020). The abundance found from the spectral modeling in this work is significantly lower than expected from the metallicity estimations from *Gaia* DR3, TIC-8 or APOGEE-2 SDSS DR17. It is likely related to the simplicity of the spectral model used in this work: as noted in Güdel (2004), the low-resolution X-ray spectra are better described by the 2-temperature plasma models (for example, *apec + apec* XSPEC model) or models with continuous power law emission measure-temperature distribution (for example, *cempow* XSPEC model). In our case, however, the statistics did not allow for accurate parameter estimations with more complicated models. For example, fitting the quiescent spectrum using the *cempow* with power law fixed at 1.0 incline results in the abundance estimation of  $Z/Z_\odot = 0.3^{+2.8}_{-0.2}$ .

The metallicities reported by the *Gaia* DR3, TIC-8 or APOGEE-2 SDSS DR17 are deviated from each other with the biggest outlier being the *Gaia* DR3 with significantly sub-Solar  $[M/H] = -0.232 \pm 0.007$ . This value contradicts the hypothesis of the SRGe J021932 being a young solar-type star, as low element abundances are characteristic for the older stellar population. TIC-8 and APOGEE-2 SDSS DR17, on the contrary, show almost Solar element abundances, which is in agreement with the young star hypothesis.

### 5.2. Estimation of the rotation period

Quasi-periodic brightness modulations of the stars with observed superflares (Maehara et al., 2012, 2015, 2017) indicate the possible relation of superflare probability to the existence of huge starspots on the stellar surface. The lifetime of the starspots on solar-type stars ranges from several days to about a year (Giles et al., 2017; Namekata et al., 2019).

We searched for this variability using the open archive of Zwicky Transient Facility (Bellm et al., 2019) observations of SRGe J021932 with data in the g filter from July 2018 to November 2023. We analyzed the periodicity in the data using Lomb-Scargle periodogram (Lomb, 1976; Scargle, 1982), but did not find any significant variability.

The source SRGe J021932 was also in view by the TESS orbiting observatory (Ricker et al., 2015) during two independent observing periods.

The first is from 19.10.2018 to 14.11.2018, which fell on sector 4 with a time resolution of 1800 seconds, and the second is from 22.10.2022 to 18.11.2022 corresponding to sector 31 with a resolution of 600 seconds. The duration of observations was  $\sim 25 - 27$  days for each sector.

To search for the periodic variability of the source, the light curves available in the public domain on the MAST portal were used. Both light curves contain areas of discontinuity in the data of about 3 to 6 days duration. Therefore, the Lomb-Scargle method, which is well suited for analyzing non-uniformly distributed time series, was used to determine the period. The data analyses used PDCSAP\_FLUX fluxes, which are simple aperture photometry (SAP\_FLUX) values taking into account common instrumental effects of TESS detectors (Ricker et al., 2015).

As a result, a period of  $3.2 \pm 0.5$  days was obtained for two independent photometric series (Fig. 6). The estimation of period

accuracy is obtained from the half-width of the maximum peak on the periodogram. It is worth noting that with a photometric single measurement error of  $\sim 0.06\%$ , the scatter in the light curve is only about 0.3%. When combining data for two sectors, the period value remains unchanged within the error limits. However, it is worth considering that the photometric noise in the light curve is much higher in the 31 sector data obtained at 600-second time resolution.

### 5.3. Star spot area estimation

In addition to the search of rotational period of the star, we estimated the upper limit of the starspot area based on the amplitude of variations present in the data for both the ZTF and TESS light curves. We estimate the amplitude of variations as the difference between 95%-quartile borders observed in the apparent magnitude data, resulting in the upper limit in the amplitude of the flux variations to be  $\Delta F/F < 5.7\%$ . Following the estimation presented in the Maehara et al. (2017), we can calculate the relation of starspot area  $A_{\text{spot}}$  normalized by the area of solar hemisphere  $A_{1/2\odot} = 3 \times 10^{32} \text{ cm}^2$  as:

$$\frac{A_{\text{spot}}}{A_{1/2\odot}} = \left(\frac{R_{\text{star}}}{R_{\odot}}\right)^2 \times \frac{T_{\text{star}}^4}{T_{\text{star}}^4 - T_{\text{spot}}^4} \times \frac{\Delta F}{F} \quad (2)$$

where  $R_{\text{star}}$  and  $R_{\odot}$  are radii of the star and the Sun, respectively,  $T_{\text{star}}$  is an effective temperature of the star,  $T_{\text{spot}}$  is an effective temperature of the starspot, calculated as

$$T_{\text{spot}} = 0.751 \times T_{\text{star}} - 3.58 \times 10^{-5} \times T_{\text{star}}^2 + 808 \quad (3)$$

The resulting upper limit estimate for the starspot area of the star from Eq. 2 is  $A_{\text{spot}}/A_{1/2\odot} < 8\%$  for the ZTF data, which is in agreement with the observation of a large sample of G-stars with superflares from (Maehara et al., 2017).

Based on the 0.3% light-curve scatter of TESS data, we can estimate the upper limit on the observed starspot area as  $A_{\text{spot}}/A_{1/2\odot} < 0.4\%$ . The observed normalized starspot area of  $< 0.4\%$  is lower compared to the typical values reported in Maehara et al. (2017) for stars with period of  $\sim 3$  days, although there are examples of the superflares observed on stars with normalized starspot area of  $\sim 0.1\%$ . Despite that, further investigation of optical brightness modulation with lower uncertainties is required to estimate the starspot area.

### 5.4. Luminosity-rotational period relation

Another possible source of information is the relation  $L_{\text{X}}/L_{\text{bol}} - P_{\text{rot}}$  shown in Fig. 7 that can be used to determine, if the star is observed in X-ray saturated state (Pizzolato et al., 2003; Wright et al., 2011). The unabsorbed X-ray luminosity of the quiescent star is estimated as  $L_{\text{XQ}} = (1.5 \pm 0.4) \times 10^{29} \text{ erg s}^{-1}$  in 0.3–4.5 keV. For the direct comparison with the existing samples, we scaled the luminosity to the ROSAT typical energy range of 0.1–2.4 keV used in (Wright et al., 2011), resulting in  $L_{\text{X}} = (1.8 \pm 0.5) \times 10^{29} \text{ erg s}^{-1}$ . The bolometric luminosity of the star from *Gaia* is  $L_{\text{bol}} = 1.19 \pm 0.04 L_{\odot}$ . Thus, the relation between X-ray and bolometric luminosities is  $L_{\text{X}}/L_{\text{bol}} = (4.0 \pm 1.1) \times 10^{-5}$ .

Based on the TESS light-curve analysis, we estimate the rotation period as  $3.2 \pm 0.5$  days. Additionally, considering the  $v \sin i = 6.1 \text{ km s}^{-1}$  based on the APOGEE-2 data and *Gaia* estimation for the radius  $R = 1.04 \pm 0.01 R_{\odot}$ , we can calculate the upper limit for the rotational period:  $P_{\text{rot}} < 9.3$  days.

The resulting position of the SRGe J021932 on the  $L_{\text{X}}/L_{\text{bol}} - P_{\text{rot}}$  diagram is overplotted on Fig. 7. This position aligns well with both the given empirical relation for the full sample and the subsample of G-type stars. Additionally, it is evident that SRGe J021932 was observed in a non-saturated state, that is describing the plateau at a  $L_{\text{X}}/L_{\text{bol}} \sim 10^{-3}$ .

### 5.5. Binary system hypothesis interpretation

In the above sections, we mainly presented the interpretation of the results for single star hypothesis. As we mentioned in Section 2.2, however, there are at least two indicators for the radial velocity variations present in *Gaia* DR3 and APOGEE-2 SDSS DR17 catalog data. Thus, it is necessary to suggest an alternative interpretation in case we are working with the data from a binary system.

One possible solution to the observed data is the binary system of G-type and M-type dwarfs, in which case the optical and IR data might have not detected the M-type companion due to 1-2 orders of magnitude lower optical luminosity. The X-ray luminosity of the M-type companion, however, can be of the  $\sim 10^{29} \text{ erg s}^{-1}$  (Magaudda et al., 2020) which would be in agreement with the observed X-ray data. The superflaring activity then would also be associated with the M-type companion, which would satisfy the common trend stated by Karmakar et al. (2022).

Rejection of either of the presented hypotheses requires additional regular observations to better determine the radial velocity variations, to search for possible eclipsing events, or to identify the companion using e.g. characteristic lines in IR spectra of the object.

## 6. Conclusion

In this work we studied the X-ray source SRGe J021932, that we associated with an X-ray active star of spectral class G2V–G4V and the rotational period  $P_{\text{rot}} < 9.3$  days.

SRGe J021932 was detected by *SRG/eROSITA* during the eUDS X-ray survey in 2019. The observed flux, however, turned out to be much dimmer compared to that reported in *XMM-Newton* catalogue 4XMM-DR12. Detailed analysis revealed that *XMM-Newton* captured the source during a flaring event on January 1 2017.

The analysis of the *XMM-Newton* light curve showed that the X-ray flare can be described by the Gaussian rise and exponential decay with characteristic scale  $\sim 400$  s and  $\sim 1300$  s, respectively.

In the X-ray spectral analysis, aside from the flare event, SRGe J021932 shows no outstanding features in its quiescent state with  $L_{\text{XQ}} = (1.4 \pm 0.4) \times 10^{29} \text{ erg s}^{-1}$  in 0.3–4.5 keV, well aligning with the sample of X-ray active G-dwarfs. The spectrum is well fitted with the one-temperature plasma emission model (APEC) with the estimated temperature of  $\sim 10$  MK.

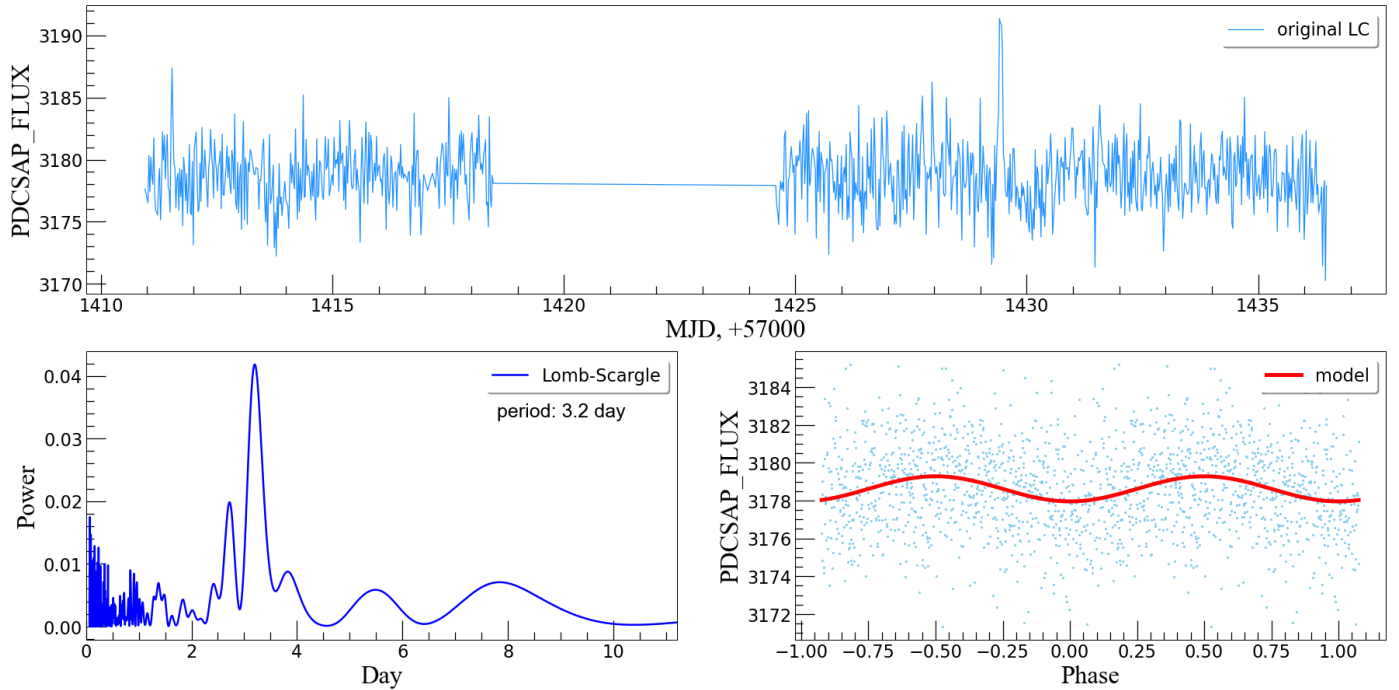


Figure 6: The top panel shows the SRGe J021932 light curve for the sector 4 data. The bottom panel shows the periodogram and phase light curve. Red colour – Lomb-Scargle model corresponding to the period of 3.2 days.

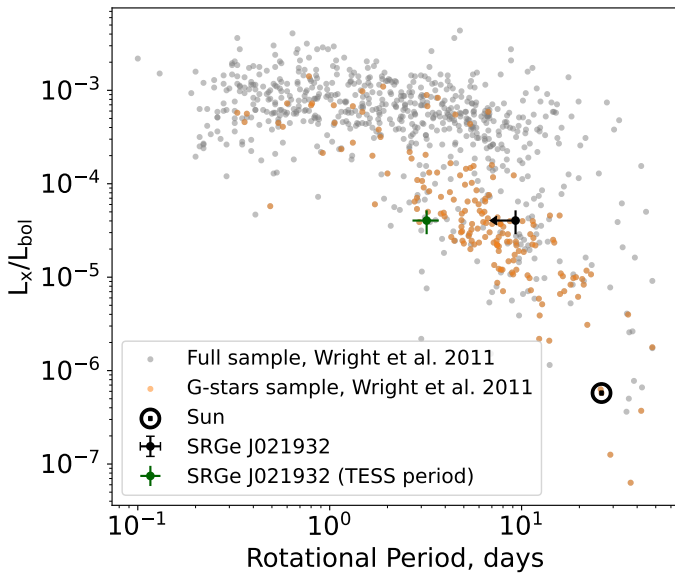


Figure 7:  $L_x/L_{\text{bol}}$  to Period relation for a sample of the stars from (Wright et al., 2011). The estimated X-ray luminosity of SRGe J021932 is recalculated to 0.1–2.4 keV to match the data of the sample. Grey dots show the full sample of the objects (824 F-M type stars), orange dots show the subsample of G-type stars (166 stars), black circle shows the Sun. The black cross shows the SRGe J021932 in a quiescent state with the 90% confidence interval errorbar and upper limit on the rotational period from APOGEE–2 data. The green cross shows the SRGe J021932 with the period estimated from the TESS data.

The spectral analysis of the flaring state showed that the flare spectrum can also be described with the one-temperature plasma emission model (APEC) with the estimated temperature of  $\sim 40$  MK. The luminosity of the observed flare is  $L_{\text{XF}} = (5.5 \pm 0.6) \times 10^{30}$  erg s $^{-1}$  in 0.3–4.5 keV. The total energy emission during the flare exceeds the canonical threshold of  $10^{33}$  erg, so we classify the observed event as a superflare on a solar-type star.

The estimated relation of X-ray luminosity to bolometric luminosity implies the SRGe J021932 to be in a non-saturated state. The analysis of Zwicky Transient Facility data was used to calculate the upper limit on the starspot area to be  $A_{\text{spot}}/A_{1/2\odot} < 8\%$ .

The analysis of TESS light-curves revealed the rotational period estimation of  $3.2 \pm 0.5$  days and a tighter upper limit on the starspot area  $A_{\text{spot}}/A_{1/2\odot} < 0.4\%$ , which is lower compared to the typical values reported in the previous observations of starspots on the solar-type stars with observed superflares.

Additionally, we report the peculiar features observed in the radial velocity estimations presented in APOGEE-2 and *Gaia* data, which can indicate the SRGe J021932 to be a binary system. One possible interpretation of the observed superflare, in this case, would be that the binary system consists of the G-type and M-type stars, the latter of which remained undetected due to a lower optical luminosity while being responsible for the majority of X-ray flux and the superflaring activity. However, further observation of the source is required to reject either single G-star or binary system hypotheses.

## Acknowledgements

This work is based on observations with eROSITA telescope onboard SRG observatory. The SRG observatory was built by Roskosmos in the interests of the Russian Academy of Sciences represented by its Space Research Institute (IKI) in the framework of the Russian Federal Space Program, with the participation of the Deutsches Zentrum für Luft- und Raumfahrt (DLR). The SRG/eROSITA X-ray telescope was built by a consortium of German Institutes led by MPE, and supported by DLR. The SRG spacecraft was designed, built, launched and is operated by the Lavochkin Association and its subcontractors. The science data are downlinked via the Deep Space Network Antennae in Bear Lakes, Ussurijsk, and Baykonur, funded by Roskosmos. The eROSITA data used in this work were processed using the eSASS software system developed by the German eROSITA consortium and proprietary data reduction and analysis software developed by the Russian eROSITA Consortium. Based on observations obtained with XMM-Newton, an ESA science mission with instruments and contributions directly funded by ESA Member States and NASA. Based on observations obtained with the Zwicky Transient Facility project. This paper includes data collected by the TESS missions and obtained from the MAST data archive at the Space Telescope Science Institute (STScI). Funding for the TESS mission is provided by the NASA Explorer Program.

The work of IB, MG, IKh supported in part by the RSF grant N 23-12-00292 (source binarity analysis based on TESS photometry, SDSS and GAIA spectroscopy data)

## Data Availability

*XMM-Newton* data have been obtained through the XMM-Newton Science Archive. ZTF data have been obtained through the NASA IPAC Infrared Science Archive. TESS data have been obtained through the Mikulski Archive for Space Telescopes at the Space Telescope Science Institute (STScI). SRG/eROSITA spectrum published in this paper can be made available upon a reasonable request.

## References

- Abdurro'uf, Accetta, K., Aerts, C., Silva Aguirre, V., Ahumada, R., Ajgaonkar, N., Filiz Ak, N., Alam, S., Allende Prieto, C., Almeida, A., Anders, F., Anderson, S.F., Andrews, B.H., Anguiano, B., Aquino-Ortíz, E., Aragón-Salamanca, A., Argudo-Fernández, M., Ata, M., Aubert, M., Avila-Reese, V., Badenes, C., Barbá, R.H., Barger, K., Barrera-Ballesteros, J.K., Beaton, R.L., Beers, T.C., Belfiore, F., Bender, C.F., Bernardi, M., Bershadsky, M.A., Beutler, F., Bidin, C.M., Bird, J.C., Bizyaev, D., Blanc, G.A., Blanton, M.R., Boardman, N.F., Bolton, A.S., Boquien, M., Borissova, J., Bovy, J., Brandt, W.N., Brown, J., Brownstein, J.R., Brusa, M., Buchner, J., Bundy, K., Burchett, J.N., Bureau, M., Burgasser, A., Cabang, T.K., Campbell, S., Cappellari, M., Carlberg, J.K., Wanderley, F.C., Carrera, R., Cash, J., Chen, Y.P., Chen, W.H., Cherinka, B., Chiappini, C., Choi, P.D., Chojnowski, S.D., Chung, H., Clerc, N., Cohen, R.E., Comerford, J.M., Comparat, J., da Costa, L., Covey, K., Crane, J.D., Cruz-Gonzalez, I., Culhane, C., Cunha, K., Dai, Y.S., Damke, G., Darling, J., Davidson, James W., J., Davies, R., Dawson, K., De Lee, N., Diamond-Stanic, A.M., Cano-Díaz, M., Sánchez, H.D., Donor, J., Duckworth, C., Dwelly, T., Eisenstein, D.J., Elsworth, Y.P., Emsellem, E., Eracleous, M., Escoffier, S., Fan, X., Farr, E., Feng, S., Fernández-Trincado, J.G., Feuillet, D., Filipp, A., Fillingham, S.P., Frinchaboy, P.M., Fromenteau, S., Galbany, L., García, R.A., García-Hernández, D.A., Ge, J., Geisler, D., Gelfand, J., Géron, T., Gibson, B.J., Goddy, J., Godoy-Rivera, D., Grabowski, K., Green, P.J., Greener, M., Grier, C.J., Griffith, E., Guo, H., Guy, J., Hadjara, M., Harding, P., Hasselquist, S., Hayes, C.R., Hearty, F., Hernández, J., Hill, L., Hogg, D.W., Holtzman, J.A., Horta, D., Hsieh, B.C., Hsu, C.H., Hsu, Y.H., Huber, D., Huertas-Company, M., Hutchinson, B., Hwang, H.S., Ibarra-Medel, H.J., Chitham, J.I., Ilha, G.S., Imig, J., Jaekle, W., Jayasinghe, T., Ji, X., Johnson, J.A., Jones, A., Jönsson, H., Katkov, I., Khalatyan, Arman, D., Kinemuchi, K., Kisku, S., Knappen, J.H., Kneib, J.P., Kollmeier, J.A., Kong, M., Kounkel, M., Kreckel, K., Krishnarao, D., Lacerna, I., Lane, R.R., Langhin, R., Lavender, R., Law, D.R., Lazar, D., Leung, H.W., Leung, H.H., Lewis, H.M., Li, C., Li, R., Lian, J., Liang, F.H., Lin, L., Lin, Y.T., Lin, S., Lintott, C., Long, D., Longa-Peñá, P., López-Cobá, C., Lu, S., Lundgren, B.F., Luo, Y., Mackereth, J.T., de la Macorra, A., Mahadevan, S., Majewski, S.R., Manchado, A., Mandeville, T., Maraston, C., Margalef-Bentabol, B., Masseron, T., Masters, K.L., Mathur, S., McDermid, R.M., McKay, M., Merloni, A., Merrifield, M., Meszaros, S., Miglio, A., Di Mille, F., Minniti, D., Minsley, R., Monachesi, A., Moon, J., Mosser, B., Mulchaey, J., Muna, D., Muñoz, R.R., Myers, A.D., Myers, N., Nadathur, S., Nair, P., Nandra, K., Neumann, J., Newman, J.A., Nidever, D.L., Nikakhtar, F., Nitschelm, C., O'Connell, J.E., Garma-Oehmichen, L., Luan Souza de Oliveira, G., Olney, R., Oravetz, D., Ortigoza-Urdaneta, M., Osorio, Y., Otter, J., Pace, Z.J., Padilla, N., Pan, K., Pan, H.A., Parikh, T., Parker, J., Peirani, S., Peña Ramírez, K., Penny, S., Percival, W.J., Perez-Fournon, I., Pinsonneault, M., Poidevin, F., Poovelil, V.J., Price-Whelan, A.M., Bárbara de Andrade Queiroz, A., Raddick, M.J., Ray, A., Rembold, S.B., Riddle, N., Riffel, R.A., Riffel, R., Rix, H.W., Robin, A.C., Rodríguez-Puebla, A., Roman-Lopes, A., Román-Zúñiga, C., Rose, B., Ross, A.J., Rossi, G., Rubin, K.H.R., Salvato, M., Sánchez, S.F., Sánchez-Gallego, J.R., Sanderson, R., Santana Rojas, F.A., Sarceno, E., Sarmiento, R., Sayres, C., Sazonova, E., Schaefer, A.L., Schiavon, R., Schlegel, D.J., Schneider, D.P., Schultheis, M., Schwore, A., Serenelli, A., Serna, J., Shao, Z., Shapiro, G., Sharma, A., Shen, Y., Shetrone, M., Shu, Y., Simon, J.D., Skrutskie, M.F., Smethurst, R., Smith, V., Sobek, J., Spoo, T., Sprague, D., Stark, D.V., Stassun, K.G., Steinmetz, M., Stello, D., Stone-Martinez, A., Storch-Bergmann, T., Stringfellow, G.S., Stutz, A., Su, Y.C., Taghizadeh-Popp, M., Talbot, M.S., Tayar, J., Telles, E., Teske, J., Thakar, A., Theissen, C., Tkachenko, A., Thomas, D., Tojeiro, R., Hernandez Toledo, H., Troup, N.W., Trump, J.R., Trussler, J., Turner, J., Tuttle, S., Unda-Sanzana, E., Vázquez-Mata, J.A., Valentini, M., Valenzuela, O., Vargas-González, J., Vargas-Magaña, M., Alfaro, P.V., Villanova, S., Vincenzo, F., Wake, D., Warfield, J.T., Washington, J.D., Weaver, B.A., Weijmans, A.M., Weinberg, D.H., Weiss, A., Westfall, K.B., Wild, V., Wilde, M.C., Wilson, J.C., Wilson, R.F., Wilson, M., Wolf, J., Wood-Vasey, W.M., Yan, R., Zamora, O., Zasowski, G., Zhang, K., Zhao, C., Zheng, Z., Zheng, Z., Zhu, K., 2022. The Seventeenth Data Release of the Sloan Digital Sky Survey: Complete Release of MaNGA, MaStar, and APOGEE-2 Data. *ApJS* 259, 35. doi:10.3847/1538-4365/ac4414, arXiv:2112.02026.
- Arnaud, K.A., 1996. XSPEC: The First Ten Years, in: Jacoby, G.H., Barnes, J. (Eds.), *Astronomical Data Analysis Software and Systems V*, p. 17.
- Audard, M., Güdel, M., Drake, J.J., Kashyap, V.L., 2000. Extreme-Ultraviolet Flare Activity in Late-Type Stars. *ApJ* 541, 396–409. doi:10.1086/309426, arXiv:astro-ph/0005062.
- Bellm, E.C., Kulkarni, S.R., Graham, M.J., Dekany, R., Smith, R.M., Riddle, R., Masci, F.J., Helou, G., Prince, T.A., Adams, S.M., Barbarino, C., Barlow, T., Bauer, J., Beck, R., Belicki, J., Biswas, R., Blagorodnova, N., Bodewits, D., Bolin, B., Brinnel, V., Brooke, T., Bue, B., Bulla, M., Burruß, R., Cenko, S.B., Chang, C.K., Connolly, A., Coughlin, M., Cromer, J., Cunningham, V., De, K., Delacroix, A., Desai, V., Duev, D.A., Eadie, G., Farnham, T.L., Feeney, M., Feindt, U., Flynn, D., Franckowiak, A., Frederick, S., Fremling, C., Gal-Yam, A., Gezari, S., Giomi, M., Goldstein, D.A., Golkhou, V.Z., Goobar, A., Groom, S., Hacopians, E., Hale, D., Henning, J., Ho, A.Y.Q., Hover, D., Howell, J., Hung, T., Huppenkothen, D., Imel, D., Ip, W.H., Ivezić, Ž., Jackson, E., Jones, L., Juric, M., Kasliwal, M.M., Kaspi, S., Kaye, S., Kelley, M.S.P., Kowalski, M., Kramer, E., Kupfer, T., Landry, W., Laher, R.R., Lee, C.D., Lin, H.W., Lin, Z.Y., Lunnan, R., Giomi, M., Mahabal, A., Mao, P., Miller, A.A., Monkewitz, S., Murphy, P., Ngeow, C.C., Nordin, J., Nugent, P., Ofek, E., Patterson, M.T., Penprase, B., Porter, M., Rauch, L., Rebba Pragada, U., Reiley, D., Rigault, M., Rodriguez, H., van

- Roestel, J., Rusholme, B., van Santen, J., Schulze, S., Shupe, D.L., Singer, L.P., Soumagnac, M.T., Stein, R., Surace, J., Sollerman, J., Szkody, P., Taddia, F., Terek, S., Van Sistine, A., van Velzen, S., Vestrand, W.T., Walters, R., Ward, C., Ye, Q.Z., Yu, P.C., Yan, L., Zolkower, J., 2019. The Zwicky Transient Facility: System Overview, Performance, and First Results. *PASP* 131, 018002. doi:10.1088/1538-3873/aaecbe, arXiv:1902.01932.
- Benz, A.O., Güdel, M., 2010. Physical Processes in Magnetically Driven Flares on the Sun, Stars, and Young Stellar Objects. *ARA&A* 48, 241–287. doi:10.1146/annurev-astro-082708-101757.
- Blanton, M.R., Bershadsky, M.A., Abolfathi, B., Albareti, F.D., Allende Prieto, C., Almeida, A., Alonso-García, J., Anders, F., Anderson, S.F., Andrews, B., Aquino-Ortíz, E., Aragón-Salamanca, A., Argudo-Fernández, M., Armengaud, E., Aubourg, E., Avila-Reese, V., Badenes, C., Bailey, S., Barger, K.A., Barrera-Ballesteros, J., Bartosz, C., Bates, D., Baumgartner, F., Bautista, J., Beaton, R., Beers, T.C., Belfiore, F., Bender, C.F., Berlind, A.A., Bernardi, M., Beutler, F., Bird, J.C., Bizyaev, D., Blanc, G.A., Blomqvist, M., Bolton, A.S., Boquien, M., Borissova, J., van den Bosch, R., Bovy, J., Brandt, W.N., Brinkmann, J., Brownstein, J.R., Bundy, K., Burgress, A.J., Burtin, E., Busca, N.G., Cappellari, M., Delgado Carigi, M.L., Carlberg, J.K., Carnero Rosell, A., Carrera, R., Chanover, N.J., Cherinka, B., Cheung, E., Gómez Maqueo Chew, Y., Chiappini, C., Choi, P.D., Chojnowski, D., Chuang, C.H., Chung, H., Cirolini, R.F., Clerc, N., Cohen, R.E., Comparat, J., da Costa, L., Cousinou, M.C., Covey, K., Crane, J.D., Croft, R.A.C., Cruz-Gonzalez, I., Garrido Cuadra, D., Cunha, K., Damke, G.J., Darling, J., Davies, R., Dawson, K., de la Macorra, A., Dell'Agli, F., De Lee, N., Delubac, T., Di Mille, F., Diamond-Stanic, A., Cano-Díaz, M., Donor, J., Downes, J.J., Drory, N., du Mas des Bourboux, H., Duckworth, C.J., Dwelly, T., Dyer, J., Ebelke, G., Eigenbrot, A.D., Eisenstein, D.J., Emsellem, E., Eracleous, M., Escoffier, S., Evans, M.L., Fan, X., Fernández-Alvar, E., Fernandez-Trincado, J.G., Feuillet, D.K., Finoguenov, A., Fleming, S.W., Font-Ribera, A., Fredrickson, A., Freischlad, G., Frinchaboy, P.M., Fuentes, C.E., Galbany, L., García-Díaz, R., García-Hernández, D.A., Gaulme, P., Geisler, D., Gelfand, J.D., Gil-Marín, H., Gillespie, B.A., Goddard, D., Gonzalez-Perez, V., Grabowski, K., Green, P.J., Grier, C.J., Gunn, J.E., Guo, H., Guy, J., Hagen, A., Hahn, C., Hall, M., Harding, P., Hasselquist, S., Hawley, S.L., Hearty, F., Gonzalez Hernández, J.I., Ho, S., Hogg, D.W., Holley-Bockelmann, K., Holtzman, J.A., Holzer, P.H., Huehnerhoff, J., Hutchinson, T.A., Hwang, H.S., Ibarra-Medel, H.J., da Silva Ilha, G., Ivans, I.I., Ivory, K., Jackson, K., Jensen, T.W., Johnson, J.A., Jones, A., Jönsson, H., Jullo, E., Kamble, V., Kinemuchi, K., Kirkby, D., Kitaura, F.S., Klaene, M., Knapp, G.R., Kneib, J.P., Kollmeier, J.A., Lacerna, I., Lane, R.R., Lang, D., Law, D.R., Lazear, D., Lee, Y., Le Goff, J.M., Liang, F.H., Li, C., Li, H., Lian, J., Lima, M., Lin, L., Lin, Y.T., Bertran de Lis, S., Liu, C., de Icaza Lizaola, M.A.C., Long, D., Lucatello, S., Lundgren, B., MacDonald, N.K., Deconto Machado, A., MacLeod, C.L., Mahadevan, S., Geimba Maia, M.A., Maiolino, R., Majewski, S.R., Malanushenko, E., Malanushenko, V., Manchado, A., Mao, S., Maraston, C., Marques-Chaves, R., Masseron, T., Masters, K.L., McBride, C.K., McDermid, R.M., McGrath, B., McGreer, I.D., Medina Peña, N., Melendez, M., Merloni, A., Merrifield, M.R., Meszaros, S., Meza, A., Minchev, I., Minniti, D., Miyaji, T., More, S., Mulchaey, J., Müller-Sánchez, F., Muna, D., Munoz, R.R., Myers, A.D., Nair, P., Nandra, K., Correa do Nascimento, J., Negrete, A., Ness, M., Newman, J.A., Nichol, R.C., Nidever, D.L., Nitschelm, C., Ntelis, P., O'Connell, J.E., Oelkers, R.J., Oravetz, A., Oravetz, D., Pace, Z., Padilla, N., Palanque-Delabrouille, N., Alonso Palicio, P., Pan, K., Parejko, J.K., Parikh, T., Páris, I., Park, C., Patten, A.Y., Peirani, S., Pellejero-Ibanez, M., Penny, S., Percival, W.J., Perez-Fournon, I., Petitjean, P., Pieri, M.M., Pinsonneault, M., Pisani, A., Poleski, R., Prada, F., Prakash, A., Queiroz, A.B.d.A., Raddick, M.J., Raichoor, A., Barboza Rembold, S., Richstein, H., Riffel, R.A., Riffel, R., Rix, H.W., Robin, A.C., Rockosi, C.M., Rodríguez-Torres, S., Roman-Lopes, A., Román-Zúñiga, C., Rosado, M., Ross, A.J., Rossi, G., Ruan, J., Ruggeri, R., Rykoff, E.S., Salazar-Albornoz, S., Salvato, M., Sánchez, A.G., Aguado, D.S., Sánchez-Gallego, J.R., Santana, F.A., Santiago, B.X., Sayres, C., Schiavon, R.P., da Silva Schimoia, J., Schlafly, E.F., Schlegel, D.J., Schneider, D.P., Schultheis, M., Schuster, W.J., Schwone, A., Seo, H.J., Shao, Z., Shen, S., Shetrone, M., Shull, M., Simon, J.D., Skinner, D., Skrutskie, M.F., Slosar, A., Smith, V.V., Sobeck, J.S., Sobreira, F., Somers, G., Souto, D., Stark, D.V., Stassun, K., Stauffer, F., Steinmetz, M., Storchi-Bergmann, T., Streblyanska, A., Stringfellow, G.S., Suárez, G., Sun, J., Suzuki, N., Szegedi, L., Taghizadeh-Popp, M., Tang, B., Tao, C., Tayar, J., Tembe, M., Teske, J., Thakar, A.R., Thomas, D., Thompson, B.A., Tinker, J.L., Tissera, P., Tojeiro, R., Hernandez Toledo, H., de la Torre, S., Tremonti, C., Troup, N.W., Valenzuela, O., Martinez Valpuesta, I., Vargas-González, J., Vargas-Magaña, M., Vazquez, J.A., Villanova, S., Vivek, M., Vogt, N., Wake, D., Walterbos, R., Wang, Y., Weaver, B.A., Weijmans, A.M., Weinberg, D.H., Westfall, K.B., Whelan, D.G., Wild, V., Wilson, J., Wood-Vasey, W.M., Wylezalek, D., Xiao, T., Yan, R., Yang, M., Ybarra, J.E., Yèche, C., Zakamska, N., Zamora, O., Zarrouk, P., Zasowski, G., Zhang, K., Zhao, G.B., Zheng, Z., Zheng, Z., Zhou, X., Zhou, Z.M., Zhu, G.B., Zoccali, M., Zou, H., 2017. Sloan Digital Sky Survey IV: Mapping the Milky Way, Nearby Galaxies, and the Distant Universe. *AJ* 154, 28. doi:10.3847/1538-3881/aa7567, arXiv:1703.00052.
- Cash, W., 1979. Parameter estimation in astronomy through application of the likelihood ratio. *ApJ* 228, 939–947. doi:10.1088/156922.
- Chen, C.T.J., Brandt, W.N., Luo, B., Ranalli, P., Yang, G., Alexander, D.M., Bauer, F.E., Kelson, D.D., Lacy, M., Nyland, K., Tozzi, P., Vito, F., Cirasuolo, M., Gilli, R., Jarvis, M.J., Lehmer, B.D., Paolillo, M., Schneider, D.P., Shemmer, O., Smail, I., Sun, M., Tanaka, M., Vaccari, M., Vignali, C., Xue, Y.Q., Banerji, M., Chow, K.E., Häubler, B., Norris, R.P., Silverman, J.D., Trump, J.R., 2018. The XMM-SERVS survey: new XMM-Newton point-source catalogue for the XMM-LSS field. *MNRAS* 478, 2132–2163. doi:10.1093/mnras/sty1036, arXiv:1804.07763.
- Didel, S., Pandey, J.C., Srivastava, A.K., Singh, G., 2024. Study of the energetic X-ray superflares from the active fast rotator AB doradus. *MNRAS* 527, 1705–1721. doi:10.1093/mnras/stad3245, arXiv:2310.13416.
- Favata, F., Reale, F., Micela, G., Sciortino, S., Maggio, A., Matsumoto, H., 2000. An extreme X-ray flare observed on EV Lac by ASCA in July 1998. *A&A* 353, 987–997. doi:10.48550/arXiv.astro-ph/9909491, arXiv:astro-ph/9909491.
- Favata, F., Schmitt, J.H.M.M., 1999. Spectroscopic analysis of a super-hot giant flare observed on Algol by BeppoSAX on 30 August 1997. *A&A* 350, 900–916. doi:10.48550/arXiv.astro-ph/9909041, arXiv:astro-ph/9909041.
- Fender, R.P., Anderson, G.E., Osten, R., Staley, T., Rumsey, C., Grainge, K., Saunders, R.D.E., 2015. A prompt radio transient associated with a gamma-ray superflare from the young M dwarf binary DG CVn. *MNRAS* 446, L66–L70. doi:10.1093/mnrasl/sl1165, arXiv:1410.1545.
- Fletcher, L., Dennis, B.R., Hudson, H.S., Krucker, S., Phillips, K., Veronig, A., Battaglia, M., Bone, L., Caspi, A., Chen, Q., Gallagher, P., Grigis, P.T., Ji, H., Liu, W., Milligan, R.O., Temmer, M., 2011. An Observational Overview of Solar Flares. *Space Sci. Rev.* 159, 19–106. doi:10.1007/s11214-010-9701-8, arXiv:1109.5932.
- Franciosini, E., Pallavicini, R., Tagliaferri, G., 2001. BeppoSAX observation of a large long-duration X-ray flare from UX Arietis. *A&A* 375, 196–204. doi:10.1051/0004-6361:20010830.
- Fruscione, A., McDowell, J.C., Allen, G.E., Brickhouse, N.S., Burke, D.J., Davis, J.E., Durham, N., Elvis, M., Galle, E.C., Harris, D.E., Huenemoerder, D.P., Houck, J.C., Ishibashi, B., Karovska, M., Nicastro, F., Noble, M.S., Nowak, M.A., Primini, F.A., Siemiginowska, A., Smith, R.K., Wise, M., 2006. CIAO: Chandra's data analysis system, in: Silva, D.R., Doxsey, R.E. (Eds.), Society of Photo-Optical Instrumentation Engineers (SPIE) Conference Series, p. 62701V. doi:10.1117/12.671760.
- Gaia Collaboration, Prusti, T., de Bruijne, J.H.J., Brown, A.G.A., Vallenari, A., Babusiaux, C., Bailer-Jones, C.A.L., Bastian, U., Biermann, M., Evans, D.W., Eyer, L., Jansen, F., Jordi, C., Klioner, S.A., Lammers, U., Lindegren, L., Luri, X., Mignard, F., Milligan, D.J., Panem, C., Poinsignon, V., Pourbaix, D., Randich, S., Sarri, G., Sartoretti, P., Siddiqui, H.I., Soubiran, C., Valette, V., van Leeuwen, F., Walton, N.A., Aerts, C., Arenou, F., Cropper, M., Drimmel, R., Høg, E., Katz, D., Lattanzi, M.G., O'Mullane, W., Grebel, E.K., Holland, A.D., Huc, C., Passot, X., Bramante, L., Cacciari, C., Castañeda, J., Chaoul, L., Cheek, N., De Angelis, F., Fabricius, C., Guerra, R., Hernández, J., Jean-Antoine-Piccolo, A., Masana, E., Messineo, R., Mowlavi, N., Niemartowicz, K., Ordóñez-Blanco, D., Panuzzo, P., Portell, J., Richards, P.J., Riello, M., Seabroke, G.M., Tanga, P., Thévenin, F., Torra, J., Els, S.G., Gracia-Abril, G., Comoretto, G., Garcia-Reinaldos, M., Lock, T., Mercier, E., Altmann, M., Andrae, R., Astraatmadja, T.L., Bellas-Velidis, I., Benson, K., Berthier, J., Blomme, R., Busso, G., Carry, B., Cellino, A., Clementini, G., Cowell, S., Creevey, O., Cuypers, J., Davidson, M., De Ridder, J., de Torres, A., Delchambre, L., Dell'Oro, A., Ducourant, C., Frémét, Y., García-Torres, M., Gosset, E., Halbwachs, J.L., Hambly, N.C., Harrison, D.L., Hauser, M., Hestroffer, D., Hodgkin, S.T., Huckle, H.E., Hutton, A., Jasniewicz, G., Jordan, S., Kontizas, M., Korn, A.J., Lanzafame, A.C., Man-

teiga, M., Moitinho, A., Muinonen, K., Osinde, J., Pancino, E., Pauwels, T., Petit, J.M., Recio-Blanco, A., Robin, A.C., Sarro, L.M., Siopis, C., Smith, M., Smith, K.W., Sozzetti, A., Thuillot, W., van Reeven, W., Viala, Y., Abbas, U., Abreu Aramburu, A., Accart, S., Aguado, J.J., Allan, P.M., Allasia, W., Altavilla, G., Álvarez, M.A., Alves, J., Anderson, R.I., Andrei, A.H., Anglada Varela, E., Antiche, E., Antoja, T., Antón, S., Arcay, B., Atzei, A., Ayache, L., Bach, N., Baker, S.G., Balaguer-Núñez, L., Barache, C., Barata, C., Barbier, A., Barblan, F., Baroni, M., Barrado y Navascués, D., Barros, M., Barstow, M.A., Becciani, U., Bellazzini, M., Bellei, G., Bello García, A., Belokurov, V., Bendjoya, P., Berihuete, A., Bianchi, L., Bienaymé, O., Billebaud, F., Blagorodnova, N., Blanco-Cuaresma, S., Boch, T., Bombrun, A., Borrachero, R., Bouquillon, S., Bourda, G., Bouy, H., Bragaglia, A., Breddels, M.A., Brouillet, N., Brüsemeister, T., Bucciarelli, B., Budnik, F., Burgess, P., Burgon, R., Burlacu, A., Busonero, D., Buzzi, R., Caffau, E., Cambras, J., Campbell, H., Cancellerie, R., Cantat-Gaudin, T., Carlucci, T., Carrasco, J.M., Castellani, M., Charlot, P., Charnas, J., Charvet, P., Chassat, F., Chiavassa, A., Clotet, M., Cocozza, G., Collins, R.S., Collins, P., Costigan, G., Crifo, F., Cross, N.J.G., Crosta, M., Crowley, C., Dafonte, C., Damerdji, Y., Dapergolas, A., David, P., David, M., De Cat, P., de Felice, F., de Laverny, P., De Luise, F., De March, R., de Martino, D., de Souza, R., Debosscher, J., del Pozo, E., Delbo, M., Delgado, A., Delgado, H.E., di Marco, F., Di Matteo, P., Diakite, S., Distefano, E., Dolding, C., Dos Anjos, S., Drazinos, P., Durán, J., Dzigan, Y., Ecale, E., Edvardsson, B., Enke, H., Erdmann, M., Escolar, D., Espina, M., Evans, N.W., Eynard Bontemps, G., Fabre, C., Fabrizio, M., Faigler, S., Falcão, A.J., Farràs Casas, M., Faye, F., Federici, L., Fedorets, G., Fernández-Hernández, J., Fernique, P., Fienga, A., Figueras, F., Filippi, F., Findeisen, K., Fonti, A., Fouesneau, M., Fraile, E., Fraser, M., Fuchs, J., Furnell, R., Gai, M., Galletti, S., Galluccio, L., Garabato, D., García-Sedano, F., Garé, P., Garofalo, A., Garralda, N., Gavras, P., Gerssen, J., Geyer, R., Gilmore, G., Girona, S., Giuffrida, G., Gomes, M., González-Marcos, A., González-Núñez, J., González-Vidal, J.J., Granvik, M., Guerrier, A., Guillout, P., Guiraud, J., Gúrpide, A., Gutiérrez-Sánchez, R., Guy, L.P., Haigron, R., Hatzidimitriou, D., Haywood, M., Heiter, U., Helmi, A., Hobbs, D., Hofmann, W., Holl, B., Holland, G., Hunt, J.A.S., Hypki, A., Icardi, V., Irwin, M., Jevardat de Fombelle, G., Jofré, P., Jonker, P.G., Jorissen, A., Julbe, F., Karampelas, A., Kochoska, A., Kohley, R., Kolenberg, K., Kontizas, E., Koposov, S.E., Kor-dopatis, G., Kousky, P., Kowalczyk, A., Krone-Martins, A., Kudryashova, M., Kull, I., Bachchan, R.K., Lacoste-Seris, F., Lanza, A.F., Lavigne, J.B., Le Poncin-Lafitte, C., Lebreton, Y., Lebzelter, T., Leccia, S., Leclerc, N., Lecoeur-Taibi, I., Lemaitre, V., Lenhardt, H., Leroux, F., Liao, S., Licata, E., Lindstrøm, H.E.P., Lister, T.A., Livanou, E., Lobel, A., Löffler, W., López, M., Lopez-Lozano, A., Lorenz, D., Loureiro, T., MacDonald, I., Magalhães Fernandes, T., Managau, S., Mann, R.G., Mantelet, G., Marchal, O., Marchant, J.M., Marconi, M., Marie, J., Marinoni, S., Marrese, P.M., Marschalkó, G., Marshall, D.J., Martín-Fleitas, J.M., Martino, M., Mary, N., Matijević, G., Mazeh, T., McMillan, P.J., Messina, S., Mestre, A., Micha-lik, D., Millar, N.R., Miranda, B.M.H., Molina, D., Molinaro, R., Molinaro, M., Molnár, L., Moniez, M., Montegriffo, P., Monteiro, D., Mor, R., Mora, A., Morbidelli, R., Morel, T., Morgenthaler, S., Morley, T., Morris, D., Mulone, A.F., Muraveva, T., Musella, I., Narbonne, J., Nelemans, G., Nicas-tro, L., Noval, L., Ordénovic, C., Ordieres-Meré, J., Osborne, P., Pagani, C., Pagano, I., Pailler, F., Palacin, H., Palaversa, L., Parsons, P., Paulsen, T., Pecoraro, M., Pedrosa, R., Pentikäinen, H., Pereira, J., Pichon, B., Piersimoni, A.M., Pineau, F.X., Plachy, E., Plum, G., Poujoulet, E., Prša, A., Pulone, L., Ragaini, S., Rago, S., Rambaux, N., Ramos-Lerate, M., Ranalli, P., Rauw, G., Read, A., Regibo, S., Renk, F., Reylé, C., Ribeiro, R.A., Rimoldini, L., Ripepi, V., Riva, A., Rixon, G., Roelens, M., Romero-Gómez, M., Rowell, N., Royer, F., Rudolph, A., Ruiz-Dern, L., Sadowski, G., Sagristà Sellés, T., Sahlmann, J., Salgado, J., Salguero, E., Sarasso, M., Savietto, H., Schnorhk, A., Schultheis, M., Sciacca, E., Segol, M., Segovia, J.C., Segransan, D., Serpell, E., Shih, I.C., Smareglia, R., Smart, R.L., Smith, C., Solano, E., Solitro, F., Sordo, R., Soria Nieto, S., Souchay, J., Spagna, A., Spoto, F., Stampa, U., Steele, I.A., Steidelmüller, H., Stephenson, C.A., Stoev, H., Suess, F.F., Süveges, M., Surdej, J., Szabados, L., Szegedi-Elek, E., Tapiador, D., Taris, F., Tauran, G., Taylor, M.B., Teixeira, R., Terrett, D., Tingley, B., Trager, S.C., Turon, C., Ulla, A., Utrilla, E., Valentini, G., van Elteren, A., Van Hemelryck, E., van Leeuwen, M., Varadi, M., Vecchiato, A., Véjanoski, J., Via, T., Vicente, D., Vogt, S., Voss, H., Votruba, V., Voutsinas, S., Walmsley, G., Weiler, M., Weingrill, K., Werner, D., Wevers, T., Whitehead, G., Wyrzykowski, Ł., Yoldas, A., Źerjal, M., Zucker, S., Zurbach, C.,

Zwitter, T., Alecu, A., Allen, M., Allende Prieto, C., Amorim, A., Anglada-Escudé, G., Arsenijevic, V., Azaz, S., Balm, P., Beck, M., Bernstein, H.H., Bigot, L., Bijaoui, A., Blasco, C., Bonfigli, M., Bono, G., Boudreault, S., Bressan, A., Brown, S., Brunet, P.M., Bunclark, P., Buonanno, R., Butkevich, A.G., Carret, C., Carrion, C., Chemin, L., Chéreau, F., Corcione, L., Darmigny, E., de Boer, K.S., de Teodoro, P., de Zeeuw, P.T., Delle Luche, C., Domingues, C.D., Dubath, P., Fodor, F., Frézouls, B., Fries, A., Fustes, D., Fyfe, D., Gallardo, E., Gallegos, J., Gardiol, D., Gebran, M., Gomboc, A., Gómez, A., Grux, E., Gueguen, A., Heyrovsky, A., Hoar, J., Iannicola, G., Isasi Parache, Y., Janotto, A.M., Joliet, E., Jonckheere, A., Keil, R., Kim, D.W., Klagyivik, P., Klar, J., Knude, J., Kochukhov, O., Kolka, I., Kos, J., Kutka, A., Lainey, V., LeBouquin, D., Liu, C., Loreggia, D., Makarov, V.V., Marseille, M.G., Martayan, C., Martinez-Rubi, O., Massart, B., Meynadier, F., Mignot, S., Munari, U., Nguyen, A.T., Nordlander, T., Ocvirk, P., O'Flaherty, K.S., Olias Sanz, A., Ortiz, P., Osorio, J., Oszkiewicz, D., Ouzounis, A., Palmer, M., Park, P., Pasquato, E., Peltzer, C., Peralta, J., Pétruraud, F., Pieniluoma, T., Pigozzi, E., Poels, J., Prat, G., Prod'homme, T., Raison, F., Rebordao, J.M., Risquez, D., Rocca-Volmerange, B., Rosen, S., Ruiz-Fuertes, M.I., Russo, F., Sembay, S., Serraller Vizcaino, I., Short, A., Siebert, A., Silva, H., Sinachopoulos, D., Slezak, E., Soffel, M., Sosnowska, D., Straižys, V., ter Linden, M., Terrell, D., Theil, S., Tiede, C., Troisi, L., Tsalmantza, P., Tur, D., Vaccari, M., Vachier, F., Valles, P., Van Hamme, W., Veltz, L., Virtanen, J., Wallut, J.M., Wichmann, R., Wilkinson, M.I., Ziaeepour, H., Zschocke, S., 2016. The Gaia mission. *A&A* 595, A1. doi:10.1051/0004-6361/201629272, arXiv:1609.04153.

Gaia Collaboration, Vallenari, A., Brown, A.G.A., Prusti, T., de Bruijne, J.H.J., Arenou, F., Babusiaux, C., Biermann, M., Creevey, O.L., Ducourant, C., Evans, D.W., Eyer, L., Guerra, R., Hutton, A., Jordi, C., Klioner, S.A., Lammers, U.L., Lindegren, L., Luri, X., Mignard, F., Panem, C., Pourbaix, D., Randich, S., Sartoretti, P., Soubiran, C., Tanga, P., Walton, N.A., Bailer-Jones, C.A.L., Bastian, U., Drimmel, R., Jansen, F., Katz, D., Lattanzi, M.G., van Leeuwen, F., Bakker, J., Cacciari, C., Castañeda, J., De Angeli, F., Fabricius, C., Fouesneau, M., Frémat, Y., Galluccio, L., Guerrier, A., Heiter, U., Masana, E., Messineo, R., Mowlavi, N., Nicolas, C., Nienar-towicz, K., Pailler, F., Panuzzo, P., Riclet, F., Roux, W., Seabroke, G.M., Sordo, R., Thévenin, F., Gracia-Abril, G., Portell, J., Teyssier, D., Altman, M., Andrae, R., Audard, M., Bellas-Velidis, I., Benson, K., Berthier, J., Blomme, R., Burgess, P.W., Busonero, D., Busso, G., Cánovas, H., Carry, B., Cellino, A., Cheek, N., Clementini, G., Damerdji, Y., Davidson, M., de Teodoro, P., Nuñez Campos, M., Delchambre, L., Dell'Oro, A., Esquej, P., Fernández-Hernández, J., Fraile, E., Garabato, D., García-Lario, P., Gosset, E., Haigron, R., Halbwachs, J.L., Hambly, N.C., Harrison, D.L., Hernández, J., Hestroffer, D., Hodgkin, S.T., Holl, B., Janßen, K., Jevardat de Fombelle, G., Jordan, S., Krone-Martins, A., Lanzafame, A.C., Löffler, W., Marchal, O., Marrese, P.M., Moitinho, A., Muinonen, K., Osborne, P., Pancino, E., Pauwels, T., Recio-Blanco, A., Reylé, C., Riello, M., Rimoldini, L., Roegiers, T., Rybizki, J., Sarro, L.M., Siopis, C., Smith, M., Sozzetti, A., Utrilla, E., van Leeuwen, M., Abbas, U., Abrahám, P., Abreu Aramburu, A., Aerts, C., Aguado, J.J., Ajaj, M., Aldea-Montero, F., Altavilla, G., Álvarez, M.A., Alves, J., Anders, F., Anderson, R.I., Anglada Varela, E., Antoja, T., Baines, D., Baker, S.G., Balaguer-Núñez, L., Balbinot, E., Balog, Z., Barache, C., Barbato, D., Barros, M., Barstow, M.A., Bartolomé, S., Bassilana, J.L., Bauchet, N., Becciani, U., Bellazzini, M., Berihuete, A., Bernet, M., Bertone, S., Bianchi, L., Binnenveld, A., Blanco-Cuaresma, S., Blazere, A., Boch, T., Bombrun, A., Bossini, D., Bouquillon, S., Bragaglia, A., Bramante, L., Breedt, E., Bressan, A., Brouillet, N., Brugaletta, E., Bucciarelli, B., Burlacu, A., Butkevich, A.G., Buzzi, R., Caffau, E., Cancellerie, R., Cantat-Gaudin, T., Carballo, R., Carlucci, T., Carnerero, M.I., Carrasco, J.M., Casamiquela, L., Castellani, M., Castro-Ginard, A., Chaoul, L., Charlot, P., Chemin, L., Chiaramida, V., Chiavassa, A., Chornay, N., Comoretto, G., Contursi, G., Cooper, W.J., Cornez, T., Cowell, S., Crifo, F., Cropper, M., Crosta, M., Crowley, C., Dafonte, C., Dapergolas, A., David, M., David, P., de Laverny, P., De Luise, F., De March, R., De Ridder, J., de Souza, R., de Torres, A., del Peloso, E.F., del Pozo, E., Delbo, M., Delgado, A., Delisle, J.B., Demouchy, C., Dharmawardena, T.E., Di Matteo, P., Diakite, S., Diener, C., Distefano, E., Dolding, C., Edvardsson, B., Enke, H., Fabre, C., Fabrizio, M., Faigler, S., Fedorets, G., Fernique, P., Fienga, A., Figueras, F., Fournier, Y., Fouron, C., Fragkoudi, F., Gai, M., Garcia-Gutierrez, A., Garcia-Reinaldos, M., García-Torres, M., Garofalo, A., Gavel, A., Gavras, P., Gerlach, E., Geyer, R., Giacobbe, P., Gilmore, G., Girona, S., Giuffrida, G., Gomel, R., Gomez, A., González-Núñez, J.,

- González-Santamaría, I., González-Vidal, J.J., Granvik, M., Guillout, P., Guiraud, J., Gutiérrez-Sánchez, R., Guy, L.P., Hatzidimitriou, D., Hauser, M., Haywood, M., Helmer, A., Helmi, A., Sarmiento, M.H., Hidalgo, S.L., Hilger, T., Hładczuk, N., Hobbs, D., Holland, G., Huckle, H.E., Jardine, K., Jasniewicz, G., Jean-Antoine Piccolo, A., Jiménez-Arranz, Ó., Jorissen, A., Juaristi Campillo, J., Julbe, F., Karbevska, L., Kervella, P., Khanna, S., Konitzas, M., Kordopatis, G., Korn, A.J., Kóspál, Á., Kostrzewa-Rutkowska, Z., Kruszyńska, K., Kun, M., Laizeau, P., Lambert, S., Lanza, A.F., Lasne, Y., Le Campion, J.F., Lebreton, Y., Lebzelter, T., Leccia, S., Leclerc, N., Lecoeur-Taibi, I., Liao, S., Licata, E.L., Lindström, H.E.P., Lister, T.A., Livanou, E., Lobel, A., Lorca, A., Loup, C., Madrero Pardo, P., Magdaleno Romeo, A., Managau, S., Mann, R.G., Manteiga, M., Marchant, J.M., Marconi, M., Marcos, J., Marcos Santos, M.M.S., Marín Pina, D., Marinoni, S., Marocco, F., Marshall, D.J., Martin Polo, L., Martín-Fleitas, J.M., Marton, G., Mary, N., Masip, A., Massari, D., Mastrobuono-Battisti, A., Mazeh, T., McMillan, P.J., Messina, S., Michalik, D., Millar, N.R., Mints, A., Molina, D., Molinaro, R., Molnár, L., Monari, G., Monguió, M., Montegriffo, P., Montero, A., Mor, R., Mora, A., Morbidelli, R., Morel, T., Morris, D., Mureaveva, T., Murphy, C.P., Musella, I., Nagy, Z., Noval, L., Ocaña, F., Ogden, A., Ordenovic, C., Osinde, J.O., Pagani, C., Pagano, I., Palaversa, L., Palicio, P.A., Pallas-Quintela, L., Panahi, A., Payne-Wardenaar, S., Peñalosa Esteller, X., Penttilä, A., Pichon, B., Piersimoni, A.M., Pineau, F.X., Plachy, E., Plum, G., Poggio, E., Prša, A., Pulone, L., Racer, E., Ragaini, S., Rainer, M., Raiteri, C.M., Rambaux, N., Ramos, P., Ramos-Lerate, M., Re Fiorentin, P., Regibo, S., Richards, P.J., Rios Diaz, C., Ripepi, V., Riva, A., Rix, H.W., Rixon, G., Robichon, N., Robin, A.C., Robin, C., Roelens, M., Rogues, H.R.O., Rohrbasser, L., Romero-Gómez, M., Rowell, N., Royer, F., Ruz Mieres, D., Rybicki, K.A., Sadowski, G., Sáez Núñez, A., Sagristà Sellés, A., Sahlmann, J., Salguero, E., Samaras, N., Sanchez Gimenez, V., Sanna, N., Santoveña, R., Sarasso, M., Schultheis, M., Sciacca, E., Segol, M., Segovia, J.C., Ségransan, D., Semeux, D., Shahaf, S., Siddiqui, H.I., Siebert, A., Siltala, L., Silvelo, A., Slezak, E., Slezak, I., Smart, R.L., Snaith, O.N., Solano, E., Solitro, F., Souami, D., Souchay, J., Spagna, A., Spina, L., Spoto, F., Steele, I.A., Steidelmüller, H., Stephenson, C.A., Süveges, M., Surdej, J., Szabados, L., Szegedi-Elek, E., Taris, F., Taylor, M.B., Teixeira, R., Tolomei, L., Tonello, N., Torra, F., Torra, J., Torralba Elipe, G., Trabucchi, M., Tsounis, A.T., Turon, C., Ulla, A., Unger, N., Vailant, M.V., van Dillen, E., van Reeven, W., Vanel, O., Vecchiato, A., Viala, Y., Vicente, D., Voutsinas, S., Weiler, M., Wevers, T., Wyrzykowski, Ł., Yoldas, A., Yvard, P., Zhao, H., Zorec, J., Zucker, S., Zwitter, T., 2023. Gaia Data Release 3. Summary of the content and survey properties. *A&A* 674, A1. doi:10.1051/0004-6361/202243940, arXiv:2208.00211.
- Giles, H.A.C., Collier Cameron, A., Haywood, R.D., 2017. A Kepler study of starspot lifetimes with respect to light-curve amplitude and spectral type. *MNRAS* 472, 1618–1627. doi:10.1093/mnras/stx1931, arXiv:1707.08583.
- Guarcello, M.G., Micela, G., Sciortino, S., López-Santiago, J., Argiroffo, C., Reale, F., Flaccomio, E., Alvarado-Gómez, J.D., Antoniou, V., Drake, J.J., Pillitteri, I., Rebull, L.M., Stauffer, J., 2019. Simultaneous Kepler/K2 and XMM-Newton observations of superflares in the Pleiades. *A&A* 622, A210. doi:10.1051/0004-6361/201834370, arXiv:1901.07263.
- Güdel, M., 2004. X-ray astronomy of stellar coronae. *A&ARv* 12, 71–237. doi:10.1007/s00159-004-0023-2, arXiv:astro-ph/0406661.
- Güdel, M., Guinan, E.F., Skinner, S.L., 1997. The X-Ray Sun in Time: A Study of the Long-Term Evolution of Coronae of Solar-Type Stars. *ApJ* 483, 947–960. doi:10.1086/304264.
- Haisch, B., Strong, K.T., Rodono, M., 1991. Flares on the Sun and other stars. *ARA&A* 29, 275–324. doi:10.1146/annurev.aa.29.090191.001423.
- Hamaguchi, K., Reep, J.W., Airapetian, V., Toriumi, S., Gendreau, K.C., Arzoumanian, Z., 2023. Delayed Development of Cool Plasmas in X-Ray Flares from the Young Sun-like Star  $\kappa^1$  Ceti. *ApJ* 944, 163. doi:10.3847/1538-4357/acae8b, arXiv:2301.01377.
- HI4PI Collaboration, Ben Bekhti, N., Flöer, L., Keller, R., Kerp, J., Lenz, D., Winkel, B., Bailin, J., Calabretta, M.R., Dedes, L., Ford, H.A., Gibson, B.K., Haud, U., Janowiecki, S., Kalberla, P.M.W., Lockman, F.J., McClure-Griffiths, N.M., Murphy, T., Nakanishi, H., Pisano, D.J., Staveley-Smith, L., 2016. HI4PI: A full-sky H I survey based on EBHIS and GASS. *A&A* 594, A116. doi:10.1051/0004-6361/201629178, arXiv:1610.06175.
- Jansen, F., Lumb, D., Altieri, B., Clavel, J., Ehle, M., Erd, C., Gabriel, C., Guainazzi, M., Gondoin, P., Much, R., Munoz, R., Santos, M., Schartel, N., Texier, D., Vacanti, G., 2001. XMM-Newton observatory. I. The spacecraft and operations. *A&A* 365, L1–L6. doi:10.1051/0004-6361:20000036.
- Joye, W.A., Mandel, E., 2003. New Features of SAOImage DS9, in: Payne, H.E., Jedrzejewski, R.I., Hook, R.N. (Eds.), *Astronomical Data Analysis Software and Systems XII*, p. 489.
- Karmakar, S., Naik, S., Pandey, J.C., Savanov, I.S., 2022. AstroSat observations of long-duration X-ray superflares on active M-dwarf binary EQ Peg. *MNRAS* 509, 3247–3257. doi:10.1093/mnras/stab3099, arXiv:2111.07527.
- Karmakar, S., Naik, S., Pandey, J.C., Savanov, I.S., 2023. Swift and XMM-Newton observations of an RS CVn-type eclipsing binary SZ Psc: superflare and coronal properties. *MNRAS* 518, 900–918. doi:10.1093/mnras/stac2970, arXiv:2210.07170.
- Karmakar, S., Pandey, J.C., Airapetian, V.S., Misra, K., 2017. X-Ray Superflares on CC Eri. *ApJ* 840, 102. doi:10.3847/1538-4357/aa6cb0, arXiv:1705.06930.
- Khamitov, I.M., Bikmaev, I.F., Gilfanov, M.R., Sunyaev, R.A., Medvedev, P.S., Gorbachev, M.A., Irtuganov, E.N., 2022. Detection of AGNs and Quasars with Significant Proper Motions Based on Gaia Data in the SRG/eROSITA Catalog of X-ray Sources. *Astronomy Letters* 48, 724–734. doi:10.1134/S1063773722110081.
- Krivonos, R., Gilfanov, M., Medvedev, P., Sazonov, S., Sunyaev, R., 2024. eUDS: the SRG/eROSITA X-ray survey of the UKIDSS Ultra Deep Survey field. Catalogue of sources. *MNRAS* 528, 1264–1275. doi:10.1093/mnras/stae105, arXiv:2312.08222.
- Kuznetsov, A.A., Kolotkov, D.Y., 2021. Stellar Superflares Observed Simultaneously with Kepler and XMM-Newton. *ApJ* 912, 81. doi:10.3847/1538-4357/abf569, arXiv:2103.10866.
- Lomb, N.R., 1976. Least-Squares Frequency Analysis of Unequally Spaced Data. *Ap&SS* 39, 447–462. doi:10.1007/BF00648343.
- Maehara, H., Notsu, Y., Notsu, S., Namekata, K., Honda, S., Ishii, T.T., Nogami, D., Shibata, K., 2017. Starspot activity and superflares on solar-type stars. *PASJ* 69, 41. doi:10.1093/pasj/psx013, arXiv:1702.07141.
- Maehara, H., Shibayama, T., Notsu, S., Notsu, Y., Nagao, T., Kusaba, S., Honda, S., Nogami, D., Shibata, K., 2012. Superflares on solar-type stars. *Nature* 485, 478–481. doi:10.1038/nature11063.
- Maehara, H., Shibayama, T., Notsu, Y., Notsu, S., Honda, S., Nogami, D., Shibata, K., 2015. Statistical properties of superflares on solar-type stars based on 1-min cadence data. *Earth, Planets and Space* 67, 59. doi:10.1186/s40623-015-0217-z, arXiv:1504.00074.
- Magaudda, E., Stelzer, B., Covey, K.R., Raetz, S., Matt, S.P., Scholz, A., 2020. Relation of X-ray activity and rotation in M dwarfs and predicted time-evolution of the X-ray luminosity. *A&A* 638, A20. doi:10.1051/0004-6361/201937408, arXiv:2004.02904.
- Maggio, A., Pallavicini, R., Reale, F., Tagliaferri, G., 2000. Twin X-ray flares and the active corona of AB Dor observed with BeppoSAX. *A&A* 356, 627–642.
- Namekata, K., Airapetian, V.S., Petit, P., Maehara, H., Ikuta, K., Inoue, S., Notsu, Y., Paudel, R.R., Arzoumanian, Z., Avramova-Boncheva, A.A., Gendreau, K., Jeffers, S.V., Marsden, S., Morin, J., Neiner, C., Vidotto, A.A., Shibata, K., 2024. Multiwavelength Campaign Observations of a Young Solar-type Star, EK Draconis. I. Discovery of Prominence Eruptions Associated with Superflares. *ApJ* 961, 23. doi:10.3847/1538-4357/ad0b7c, arXiv:2311.07380.
- Namekata, K., Maehara, H., Notsu, Y., Toriumi, S., Hayakawa, H., Ikuta, K., Notsu, S., Honda, S., Nogami, D., Shibata, K., 2019. Lifetimes and Emergence/Decay Rates of Star Spots on Solar-type Stars Estimated by Kepler Data in Comparison with Those of Sunspots. *ApJ* 871, 187. doi:10.3847/1538-4357/aaf471, arXiv:1811.10782.
- Osten, R.A., Drake, S., Tueller, J., Cummings, J., Perri, M., Moretti, A., Covino, S., 2007. Nonthermal Hard X-Ray Emission and Iron  $\mathrm{K}\alpha$  Emission from a Superflare on II Pegasi. *ApJ* 654, 1052–1067. doi:10.1086/509252, arXiv:astro-ph/0609205.
- Osten, R.A., Godet, O., Drake, S., Tueller, J., Cummings, J., Krimm, H., Pye, J., Pal'shin, V., Golenetskii, S., Reale, F., Oates, S.R., Page, M.J., Melandri, A., 2010. The Mouse That Roared: A Superflare from the dMe Flare Star EV Lac Detected by Swift and Konus-Wind. *ApJ* 721, 785–801. doi:10.1088/0004-637X/721/1/785, arXiv:1007.5300.
- Pizzolato, N., Maggio, A., Micela, G., Sciortino, S., Ventura, P., 2003. The stellar activity-rotation relationship revisited: Dependence of saturated and non-saturated X-ray emission regimes on stellar mass for late-type dwarfs.

- A&A 397, 147–157. doi:10.1051/0004-6361:20021560.
- Predehl, P., Andritschke, R., Arefiev, V., Babyshkin, V., Batanov, O., Becker, W., Böhringer, H., Bogomolov, A., Boller, T., Borm, K., Bornemann, W., Bräuninger, H., Brüggen, M., Brunner, H., Brusa, M., Bulbul, E., Buntov, M., Burwitz, V., Burkert, W., Clerc, N., Churazov, E., Coutinho, D., Dauser, T., Dennerl, K., Doroshenko, V., Eder, J., Emberger, V., Eraerds, T., Finoguenov, A., Freyberg, M., Friedrich, P., Friedrich, S., Fürmetz, M., Georgakakis, A., Gilfanov, M., Granato, S., Grossberger, C., Gueguen, A., Gureev, P., Haberl, F., Häkler, O., Hartner, G., Hasinger, G., Huber, H., Ji, L., Kienlin, A.v., Kink, W., Korotkov, F., Kreykenbohm, I., Lamer, G., Lomakin, I., Lapshov, I., Liu, T., Maitra, C., Meidinger, N., Menz, B., Merlini, A., Mernik, T., Mican, B., Mohr, J., Müller, S., Nandra, K., Nazarov, V., Pacaud, F., Pavlinsky, M., Perinati, E., Pfeffermann, E., Pietschner, D., Ramos-Ceja, M.E., Rau, A., Reiffers, J., Reiprich, T.H., Robrade, J., Salvato, M., Sanders, J., Santangelo, A., Sasaki, M., Scheuerle, H., Schmid, C., Schmitt, J., Schwape, A., Shirshakov, A., Steinmetz, M., Stewart, I., Strüder, L., Sunyaev, R., Tenzer, C., Tiedemann, L., Trümper, J., Voron, V., Weber, P., Wilms, J., Yaroshenko, V., 2021. The eROSITA X-ray telescope on SRG. A&A 647, A1. doi:10.1051/0004-6361/202039313, arXiv:2010.03477.
- Pye, J.P., Rosen, S., Fyfe, D., Schröder, A.C., 2015. A survey of stellar X-ray flares from the XMM-Newton serendipitous source catalogue: HIPPARCOS-Tycho cool stars. A&A 581, A28. doi:10.1051/0004-6361/201526217, arXiv:1506.05289.
- Ricker, G.R., Winn, J.N., Vanderspek, R., Latham, D.W., Bakos, G.Á., Bean, J.L., Berta-Thompson, Z.K., Brown, T.M., Buchhave, L., Butler, N.R., Butler, R.P., Chaplin, W.J., Charbonneau, D., Christensen-Dalsgaard, J., Clampin, M., Deming, D., Doty, J., De Lee, N., Dressing, C., Dunham, E.W., Endl, M., Fressin, F., Ge, J., Henning, T., Holman, M.J., Howard, A.W., Ida, S., Jenkins, J.M., Jernigan, G., Johnson, J.A., Kaltenegger, L., Kawai, N., Kjeldsen, H., Laughlin, G., Levine, A.M., Lin, D., Lissauer, J.J., MacQueen, P., Marcy, G., McCullough, P.R., Morton, T.D., Narita, N., Paegert, M., Palle, E., Pepe, F., Pepper, J., Quirrenbach, A., Rinehart, S.A., Sasselov, D., Sato, B., Seager, S., Sozzetti, A., Stassun, K.G., Sullivan, P., Szentgyorgyi, A., Torres, G., Udry, S., Villasenor, J., 2015. Transiting Exoplanet Survey Satellite (TESS). Journal of Astronomical Telescopes, Instruments, and Systems 1, 014003. doi:10.1117/1.JATIS.1.1.014003.
- Scargle, J.D., 1982. Studies in astronomical time series analysis. II. Statistical aspects of spectral analysis of unevenly spaced data. ApJ 263, 835–853. doi:10.1086/160554.
- Schaefer, B.E., King, J.R., Deliyannis, C.P., 2000. Superflares on Ordinary Solar-Type Stars. ApJ 529, 1026–1030. doi:10.1086/308325, arXiv:astro-ph/9909188.
- Shibata, K., Isobe, H., Hillier, A., Choudhuri, A.R., Maehara, H., Ishii, T.T., Shibayama, T., Notsu, S., Notsu, Y., Nagao, T., Honda, S., Nogami, D., 2013. Can Superflares Occur on Our Sun? PASJ 65, 49. doi:10.1093/pasj/65.3.49, arXiv:1212.1361.
- Smith, R.K., Brickhouse, N.S., Liedahl, D.A., Raymond, J.C., 2001. Collisional Plasma Models with APEC/APED: Emission-Line Diagnostics of Hydrogen-like and Helium-like Ions. ApJ 556, L91–L95. doi:10.1086/322992, arXiv:astro-ph/0106478.
- Stassun, K.G., Oelkers, R.J., Paegert, M., Torres, G., Pepper, J., De Lee, N., Collins, K., Latham, D.W., Muirhead, P.S., Chittidi, J., Rojas-Ayala, B., Fleming, S.W., Rose, M.E., Tenenbaum, P., Ting, E.B., Kane, S.R., Barclay, T., Bean, J.L., Brassuer, C.E., Charbonneau, D., Ge, J., Lissauer, J.J., Mann, A.W., McLean, B., Mullally, S., Narita, N., Plavchan, P., Ricker, G.R., Sasselov, D., Seager, S., Sharma, S., Shiao, B., Sozzetti, A., Stello, D., Vanderspek, R., Wallace, G., Winn, J.N., 2019. The Revised TESS Input Catalog and Candidate Target List. AJ 158, 138. doi:10.3847/1538-3881/ab3467, arXiv:1905.10694.
- Stelzer, B., Caramazza, M., Raetz, S., Argiroffi, C., Coffaro, M., 2022. The Great Flare of 2021 November 19 on AD Leonis. Simultaneous XMM-Newton and TESS observations. A&A 667, L9. doi:10.1051/0004-6361/202244642, arXiv:2209.05068.
- Strüder, L., Briel, U., Dennerl, K., Hartmann, R., Kendziorra, E., Meidinger, N., Pfeffermann, E., Reppin, C., Aschenbach, B., Bornemann, W., Bräuninger, H., Burkert, W., Elender, M., Freyberg, M., Haberl, F., Hartner, G., Heuschmann, F., Hippmann, H., Kastelic, E., Kemmer, S., Kettenring, G., Kink, W., Krause, N., Müller, S., Oppitz, A., Pietsch, W., Popp, M., Predehl, P., Read, A., Stephan, K.H., Stötter, D., Trümper, J., Holl, P., Kemmer, J., Soltau, H., Stötter, R., Weber, U., Weichert, U., von Zanthier, C., Carathanassis, D., Lutz, G., Richter, R.H., Solc, P., Böttcher, H., Kuster, M., Staubert, R., Abbey, A., Holland, A., Turner, M., Balasini, M., Bignami, G.F., La Palombara, N., Villa, G., Buttler, W., Gianini, F., Lainé, R., Lumb, D., Dhez, P., 2001. The European Photon Imaging Camera on XMM-Newton: The pn-CCD camera. A&A 365, L18–L26. doi:10.1051/0004-6361:20000066.
- Sunyaev, R., Arefiev, V., Babyshkin, V., Bogomolov, A., Borisov, K., Buntov, M., Brunner, H., Burenin, R., Churazov, E., Coutinho, D., Eder, J., Eismont, N., Freyberg, M., Gilfanov, M., Gureev, P., Hasinger, G., Khabibullin, I., Kolmykov, V., Komovkin, S., Krivonos, R., Lapshov, I., Levin, V., Lomakin, I., Lutovinov, A., Medvedev, P., Merloni, A., Mernik, T., Mikhailov, E., Molodtsov, V., Mzhelsky, P., Müller, S., Nandra, K., Nazarov, V., Pavlinsky, M., Pogodin, A., Predehl, P., Robrade, J., Sazonov, S., Scheuerle, H., Shirshakov, A., Tkachenko, A., Voron, V., 2021. SRG X-ray orbital observatory. Its telescopes and first scientific results. A&A 656, A132. doi:10.1051/0004-6361/202141179, arXiv:2104.13267.
- Takasao, S., Mitsuishi, I., Shimura, T., Yoshida, A., Kunitomo, M., Tanaka, Y.A., Ishihara, D., 2020. Investigation of Coronal Properties of X-Ray Bright G-dwarf Stars Based on the Solar Surface Magnetic Field–Corona Relationship. ApJ 901, 70. doi:10.3847/1538-4357/abad34, arXiv:2008.04255.
- Tu, Z.L., Yang, M., Wang, H.F., Wang, F.Y., 2021. Superflares, Chromospheric Activities, and Photometric Variabilities of Solar-type Stars from the Second-year Observation of TESS and Spectra of LAMOST. ApJS 253, 35. doi:10.3847/1538-4365/abda3c, arXiv:2101.02901.
- Webb, N.A., Coriat, M., Traulsen, I., Ballet, J., Motch, C., Carrera, F.J., Koliopanos, F., Authier, J., de la Calle, I., Ceballos, M.T., Colomo, E., Chuard, D., Freyberg, M., Garcia, T., Kolehmainen, M., Lamer, G., Lin, D., Maggi, P., Michel, L., Page, C.G., Page, M.J., Perea-Calderon, J.V., Pineau, F.X., Rodriguez, P., Rosen, S.R., Santos Lleo, M., Saxton, R.D., Schwape, A., Tomás, L., Watson, M.G., Zakardjian, A., 2020. The XMM-Newton serendipitous survey. IX. The fourth XMM-Newton serendipitous source catalogue. A&A 641, A136. doi:10.1051/0004-6361/201937353, arXiv:2007.02899.
- Wright, N.J., Drake, J.J., Mamajek, E.E., Henry, G.W., 2011. The Stellar-activity-Rotation Relationship and the Evolution of Stellar Dynamos. ApJ 743, 48. doi:10.1088/0004-637X/743/1/48, arXiv:1109.4634.